Crustal Thickness Variations and their Tectonic Implications beneath the Uttarakhand Himalayas and the adjoining Tectonic Segments: Results from 3-D Tomographic Inversion of Local and Regional Earthquake Data

J. Raoof[1*], A. Tiwari[1], P. Kumar[1], and A. Paul[1]

[1] Wadia Institute of Himalayan Geology, Dehradun, 248001, Uttarakhand, India.

Corresponding author: Javed Raoof (rjavediitk@gmail.com)
Ajay Paul (ajaypaul@wihg.res.in)

Key Points:

- Variable geometry of the Moho boundary beneath the Himalayan-Tibetan Orogen
- Crustal thickness varies from ~40-65 km beneath the Himalayas and the thickest crust ~85 km lies beneath the southwest Tibet
- Evidence of subducting/underthrusting Indian plate beneath the collision boundary towards north and the subducted Tibetan slab towards south

Abstract

We image the high-resolution velocity structures of the crust and uppermost mantle beneath the western part of the Himalayan-Tibetan orogen through tomographic inversion of local and regional earthquake data. We herein reconstruct and present the tomographic image of the variable configuration of the Moho boundary beneath the Himalayan-Tibetan orogen. The thickness of the crust varies between ~40-65 km from south beneath the sub-Himalaya to north beneath the Higher Himalaya. The thickest crust imaged as thick as ~85 km, located ~100 km from ITSZ towards north beneath the southwest Tibet. Our results also report significantly variable geometry of the Moho boundary along the tectonic trend of the Himalayan-Tibetan orogen, which may indicate that the Indian plate subducted/underthrusted beneath the Eurasian plate in a piecewise manner as a consequence of differential convergence rates, counter clockwise rotation of the Indian plate and episodic collision processes. We also image the geometry of the subducting/underthrusting Indian plate beneath the Himalayan-Tibetan orogen. We present the geodynamic model of the two subducted slabs, where the Indian plate subducts/underthrusts towards north and the Tibetan slab subducted southwards beneath the Tibetan plateau. We infer that the Indian plate is torn into pieces differing in its northern limits and angle of subduction/underthrusting. Where its westernmost end subducts/underthrusts below the Eurasian plate with a gentle dip crossing ITSZ and KKMF. On the other hand, towards east the Indian plate subducts/underthrust the Eurasian plate with a relatively greater angle near ITSZ, approximately 250 km distant from HFT.

Plain Language Summary

Seismic images of the crust and uppermost mantle beneath the Himalayan-Tibetan orogen may provide an important insight into the complicated tectonic deformation mechanisms and underlying geodynamics. They may also provide an excellent opportunity to study and comprehend the responsible mechanisms for differential evolution of the Indo-Asia collision zone through geological time. Here, we reconstruct the high-resolution tomographic model for the western sector of the Himalayan-Tibetan orogen through high-resolution arrival time of local and regional earthquake data using widely implemented tomography algorithm LOTOS [Koulakov, 2009a]. We estimate the Moho depth map for the entire study area that has never been attempted before through seismic studies. We also present the tomographic evidence of along strike varying architecture of the crust as well as the Indian Lithosphere that underthrusts northward under the Himalayas and the southern Tibet. We also present evidence of the southward subducted Tibetan slab just beneath the southern Tibet. The along strike varying architecture of the crust reflects the varying deformation mechanisms and differential interactions of the geological units through geological time as a consequence of differential modes of evolutionary processes of Indo-Asia collision, several episodes of collision and rotations of the Indian plate with respect to the Eurasian plate.

1 Introduction

At ~80 Ma ago Indian plate was ~6,400 km south of the Eurasian plate but moving northwards at a very fast and episodes of accelerating/decelerating [Dewey et al., 1988; Capitanio et al., 2010; van Hinsbergen et al., 2011; Jagoutz et al., 2015] convergence rate ~14–20 cm/year [Patriat and Achache, 1984; Besse et al., 1988; Klootwijk et al., 1992; Kumar et al., 2007; Molnar and Stock, 2009; Copley et al., 2010; Cande and Stegman, 2011; van Hinsbergen et al., 2011; White and Lister, 2012] with varying vector of the movement and rotation of the

Indian Plate [Treloar and Coward, 1991], resulted in the onset of the continent–continent collision between the two plates [Le Fort, 1975; Molnar and Tapponnier, 1975; Seeber et al., 1981; England and McKenzie, 1982; Ni and Barazangi, 1984] in the past ~ 60–45 Ma [Patriat and Achache, 1984; Besse et al., 1984; Dewey et al., 1989; Tapponnier et al., 2001; DeCelles et al., 2002; Najman et al., 2010]. This gives rise to the great Himalayan–Tibetan orogen and the associated deformation mechanisms. The cause of fast and rapid anomalous convergence rate was the result of reduced viscous pressure between the subducting slabs during ~90–80 Ma, and arrival of mantle plume below the Indian plate with emplacement of large igneous province on the Indian plate, and later this fast and rapid convergence rate decayed rapidly due to the collision of the Indian Plate with the southern subducting systems at ~50 Ma [van Hinsbergen et al., 2011; Jagoutz et al., 2015; Pusok and Stegman, 2020]. The number, timing and geometry of the subduction systems have profound influence on the plate convergence rates [Jagoutz et al., 2015]. The initial geometry of the Indian plate, counterclockwise rotations, several episodes of collision [Treloar and Coward, 1991; Capitanio et al., 2015] and the acceleration/deceleration in the convergent rate [van Hinsbergen et al., 2011] also played an important role in the evolution of Indo-Asia collision zone through geological time.

The continued convergence of the Indian plate with respect to the Eurasian plate was likely accommodated by the subduction, underthrusting, shortening and thickening, extrusion/delamination, compression, faulting/thrusting [Dewey et al., 1988; Li et al., 2015; Molnar et al., 1993; Owens and Zandt, 1997; Tapponnier et al., 2001; DeCelles et al., 2002; Replumaz, et al., 2004; Replumaz et al., 2010; Guillot and Replumaz, 2013; Replumaz et al., 2013; Capitanio et al., 2015] and resulted in more complex tectonic deformation mechanisms [De Franco et al., 2008; Capitanio et al., 2015], and lithospheric process involved in the intraplate tectonics [Replumaz et al., 2013]. The total amount of convergence of about ~2000–3000 km has been taken place between the Indian and Eurasian plates [Molnar and Tapponnier, 1977; Patriat and Achache, 1984; Tapponnier et al., 1986; Le Pichon et al., 1992; Guillot et al., 2003]. The Indian continental subduction initiated at the northwestern margin of the Indian plate at ~35 ± 5 Ma along ~1500-km-long WNW–ESE striking zone (i.e., tectonic trend of the great Himalayan range), and ended up with a process of progressive slab break-off [Replumaz et al., 2010c]. The process of slab break-off started most probably ~25 Ma at the western margin of the Indian slab and then propagated eastwards until the complete slab break-off ~15 Ma. [Replumaz et al., 2010c]. The thickening of the Himalayan-Tibetan region and initiation of intra-Tibetan subduction resulted between ~45 and ~35 Ma [Guillot and Replumaz, 2013; Replumaz et al., 2014].

Several researchers reported differential amount of shortening e.g., ~1000–1400 km [Yin and Harrison [2000], ~1300 km [Replumaz et al., 2013], and ~1500 km based on a paleomagnetic study [Patzelt et al., 1996] and a tomographic study [Replumaz et al., 2004]. After the initial continental collision, the subducted Indian continental lithospheric slab broken off and a part of it got dragged down with the oceanic part before the break off event [Replumaz et al., 2010]. The subduction of the continental lithosphere to a larger depth in the mantle have been reported by several workers [van der Hilst et al., 1997; van der Voo et al., 1999]. About ~600-1,000 km of the Indian continental margin [Gaetani and Garzanti, 1991] was dragged down into the mantle, behind the sinking Tethyan oceanic lithosphere [van der Voo et al., 1999; Guillot et al., 2003; Replumaz et al., 2004], where it partly detached from the Indian plate once it reached mid-mantle depths [van der Voo et al., 1999; Replumaz et al., 2004]. Indian slab had several broke off events during the collision episode between the Indian and Eurasian plates [Replumaz et al., 2014]. The stretched Indian slab had detached from the indenting Indian plate during the collision process between the Indian and the Eurasian plates, and remained stationary back in time underneath the northward-drifting Indian plate [Husson et al., 2014]. One major breakoff occurred between the Indian plate and the Tethys Ocean at ~45 Ma [Replumaz et al., 2013, 2014]. The subduction process of high-strength Indian continental lithosphere dominates during the early Eocene (~55-45 Ma), and ended with the Indian slab breakoff [Guiillot and Replumaz, 2013]. Replumaz et al. [2014] have shown a vertical slab continuous to the continent that override the deeper detached Tethyan sab and a similar structure with a detached slab, yet closer to the Tethys slab in the central region. Between ~40 and 50% of the Indian continental crust has been recycled into the mantle by the continental subduction. While just 3% of the Asian continental crust was recycled into the mantle that corresponds to one episode of the continental subduction, occurring most probably just after the start of the collision along the Bangong suture [Replumaz et al., 2010b].

The Indian plate is still underthrusting under the Himalayan-Tibetan orogen [Ni and Barazangi, 1984; Zhou and Murphy, 2005; Replumaz et al., 2014] leading to shortening in the Himalayas, whereas further east convergence is accommodated by extrusion of Burma microplate and Andaman–Nicobar region eastward [Replumaz et al., 2014]. The geotectonic units accreted in the Himalayan-Tibetan orogen represent that ~1020 km of the Greater Indian crust has consumed [DeCelles et al., 2001], whereas ~only 515 km of the lower crust remained to be entrained into the mantle. This consumed Indian lower crust has been sunk into the mantle at depth [Mattauer, 1986; Le Pichon et al., 1992; DeCelles et al., 2001] that follows the dipping Indian lithosphere beneath the Himalayas [Kosarev et al., 1999; Wu et al., 2022].

Presently, Indian plate is moving northward at an average convergence rate of ~4–5 cm/year [DeMets et al., 1994, 2010; Paul et al., 2001; Sella et al., 2002; Copley et al., 2010], and underthrusting under the Himalayan-Tibetan orogen along a ~1000 km long, very shallow, gently dipping (0°–5°) detachment plane/decollement, referred as the Main Himalayan Thrust (MHT) that separates the subducted/underthrusted Indian plate crust with the overlying Tibetan crust [Molnar and Tapponnier, 1975; Zhao et al., 1993; Caldwell et al., 2013; Xu et al., 2017]. The Himalayan arc thrusts motion account for about ~1–2 cm/year of the total ~4-5 cm/year of convergence, whereas the remainder accounts for the thrusting, crustal extension, and strike-slip kinematics farther north within the Eurasian Plate [Freymueller et al., 1996; Bilham et al., 1997, 1998; Powers et al., 1998; Wesnousky et al., 1999; Lavé and Avouac, 2000, 2001; Kumar et al., 2001; Bilham and Ambraseys, 2005].

Many seismic imaging studies have been made in the study region and the adjoining regions during the last two decades in order to image the structure of the crust and mantle at different scales and understand the geodynamics of the region. Results derived from the previous studies have played an important role in understanding the mechanisms and the evolutionary processes of the Indo-Asian collision zone and the associated deformation mechanisms but still unable to answer few questions related to varying complicated architecture and its tectonic implications. A high-resolution image reconstructed through S-to-P converted seismic waves reveals south to north thickening of the Indian lithosphere from ~130–160 km just beneath the Himalayas to a depth of ~200–220 km beneath the Tibet just south of the Bangong suture [Kumar et al., 2006; Xu et al., 2017]. Doubling of the Asian crust during the collision is evidenced by doubling of the Moho depth beneath the Himalayan-Tibetan orogen which is found to be as deep as ~70 km [Mathews and Hirn, 1984; Kind et al., 2002; Tan et al., 2023], ~75 km [Rai et al., 2006; Gilligan et al., 2015], ~80–82 km [Royden et al., 2008; Xu et al., 2017], and up to ~90 km [Wittlinger et al., 2004; Zhang et al., 2014], beneath the southern Tibet just south of the Bangong suture.

Though previous tomographic/receiver function studies improve our understanding, but either they are local, sparse or along very few transects and therefore they are lacking in constructing and conceptualizing a generalized geodynamic model for the entire Himalayan-Tibetan orogen. Utilizing the high-resolution local and regional earthquake data, here we intend to reconstruct the high-resolution tomographic image through 3-D inversion of arrival time data with our three-fold objectives: (1) to image, investigate and study the nature and geometry of the crust-mantle boundary (Moho); (2) to image the subducting/underthrusting Indian plate under the Himalayan-Tibetan orogen and understand the geodynamics of the study region; (3) to prepare the Moho depth map for the entire area, study the lateral variations in Moho-depth and comprehend the responsible tectonic processes, and corroborate this variation with the seismogenesis in the study region (Figure 1).

Figure 1: Tectonic map of the Uttarakhand Himalayas and its adjoining tectonic segments with major tectonic features, showing epicenters of significant historical and recent large-magnitude earthquakes since 1501 CE. Red stars - epicenters of great earthquakes Mw ≥ 8 with the magnitude and year of occurrence; Cyan stars - epicenters of major earthquakes with Mw 7–8 with the magnitude and year of occurrence; Yellow dots - epicenters of earthquakes with Mw 6–7; Blue dots – epicenters of earthquakes with Mw 5–6 [Data Source: NCS; USGS; ISC; NGDC; Bilham and Ambraseys, 2005; Kumar et al., 2006, 2010; Szeliga et al., 2010; Mukhopadhyay and Dasgupta, 2013; Bungum et al., 2017; Bilham, 2019]. Arrows indicate GPS velocities in different regions along the great Himalayan arc [after Stevens and Avouac, 2015; Yadav et al., 2019]. Pink polygon shows the subducting/underthrusting Delhi-Haridwar basement Ridge [after Gahalaut and Kundu, 2012; Godin and Harris, 2014; Hetényi et al., 2016]. Abbreviations: ITSZ: Indus–Tsangpo–Suture Zone; STDS: South-Tibetan-Detachment System; MCT: Main Central Thrust; MBT: Main Boundary Thrust; HFT: Himalayan Frontal Thrust (also referred as MFT: Main Frontal Thrust); SAT: South Almora Thrust; NAT: North Almora Thrust; RGT: Ramgarh Thrust; KLT: Krol Thrust; JMT: Jwalamukhi Thrust; KKMF: Karakorum Fault; SDNF: Sunder Nagar Fault; RPMF: Ropar-Manali Fault; KSWF: Kishtwar Fault; GBF: Great Boundary Fault; MBF: Moradabad Fault; MGDF: Mahendgarh-Dehradun Fault; KK-CGR: Kaurik-Chango Rift [after Dasgupta et al., 2000; Gahalaut and Kundu, 2012; Jayangondaperumal et al., 2018; Thakur et al., 2019; Jain, 2020; Malik et al., 2023]. Background topography is shown.

2 Geotectonic Framework of the Study Region

The study region geographically lying between 27–34° N and 75–83 °E, can be broadly categorized as Uttarakhand Himalayas (also known as Garhwal–Kumaon Himalayas), Himachal Himalayas including Kangra Re–entrant and Nahan Salient regions to its west, westernmost Nepal Himalayas to its east, Ladakh Range to its northwest, southern Tibetan Plateau to its North, and Indo–Gangetic Plain (IGP) and Delhi–Haridwar Ridge (DHR) to its south (Figure 1).

The great Himalayan–Tibetan orogen can be categorized and characterized by six orogen–parallel, fault–bounded litho–tectonic zones along its entire length [Heim and Gansser, 1939; Gansser, 1964; Le Fort, 1975; Hodges, 2000; Najman and Garzanti, 2000; Yin and Harrison 2000; Jayangondaperumal et al., 2018; Thakur et al., 2019]. These zones are longitudinally separated from successively deeper crustal levels towards north [Yin, 2006; Hubbard et al., 2021] by principal intra–continental, north–dipping, crustal scale thrust faults, and all the principal thrust faults root in a mid–crustal, gently northward dipping detachment or decollement, the Main Himalayan Thrust (MHT) [Zhao et al., 1993; Nelson et al., 1996; Bilham et al., 1997; Hauck et al., 1998; Avouac, 2003; Nabelek et al., 2009; Stevens and Avouac, 2015; Thakur et al., 2019]. From south to north, major bounding faults and the classic litho–tectonic zones are: the Himalayan Frontal Thrust (HFT) also referred as Main Frontal Thrust (MFT), Sub–Himalaya (or outer Himalaya or Siwaliks), Main Boundary Thrust (MBT), Lesser Himalaya, Main Central Thrust (MCT), Greater (or Higher) Himalaya, South Tibetan Detachment System (STDS) also known as Tethyan Thrust (TT), Tethyan Himalaya (or Tibetan Himalaya), Indus–Tsangpo Suture Zone (ITSZ) delimiting the northern boundary of the Indian plate subducting/underthrusting under the Tibet, and the Trans Himalayan Zone (Figure 1) [Allégre et al., 1984; Bendick and Bilham, 2001; Burg and Chen, 1984; Chemenda et al., 2000; DeCelles et al., 2016; Gansser, 1964; He et al., 2015, 2016; Heim and Gansser, 1939; Hodges, 2000; Kohn, 2014; Le Fort, 1975; Searle and Treloar, 2019; Larson et al., 2015; Najman and Garzanti, 2000; Schelling and Arita, 1991; Srivastava and Mitra, 1994; Thakur, 1987; Thakur et al., 2019; Upreti, 1999; Valdiya, 1980; Webb et al., 2007, 2011; Yin and Harrison 2000; Yin et al., 2010]. As a result of continued convergence/collision of the Indian and Asian plates, the great Himalayan–Tibetan orogen evolved and hence the convergence accommodated as a progressive southward propagating major thrust faults system by the increasing shortening induced, in a way that the MCT activated in Early Miocene, the MBT in the Middle Miocene and the HFT in the Quaternary [Ahmad et al., 2000; Hodges 2000; Robinson et al., 2006; Thakur et al., 2019; Webb et al., 2007; Yin, 2006]. This suggests that the earliest deformation zone is preserved in the Tethyan Zone to the north, while the most recent deformation zone where most of the ongoing crustal shortening accommodated in the Sub–Himalaya is associated with the seismically active HFT [Ahmad et al., 2000; DeCelles et al. 2002; Dey et al., 2016; Godin and Harris, 2014; Jade et al., 2017; Jouanne et al., 2004; Kumar et al. 2001, 2006; Lav'e and Avouac 2000; Mugnier et al., 1999; Nakata, 1989; Thakur et al., 2019]. Shortening was substantially accommodated by movement along the MCT in the early phases of thrusting, which resulted in the uplift and erosion of the Higher Himalayan Crystalline Series as well as the deposition of the Sub–Himalayan succession in the foreland basin [Ahmad et al., 2000]. A hinterland–dipping duplex was produced by synchronous folding and faulting, which culminated in the form of out–of–sequence thrust faults [Ahmad et al., 2000].

The Sub–Himalaya (or Siwaliks): delimited by the HFT to the south and the MBT to the north, this zone is primarily comprised of foreland basin sedimentary rocks, product of Paleogene and Neogene molassic sediments eroded from early collisional topography or the rising orogen and deposited at least since 16 Ma in front of the mountain belt [Critelli and Garzanti, 1994; DeCelles et al., 1998a,1998b,2001; Harrison et al., 1993; Johnson et al., 1985; Najman and Garzanti, 2000; Najman et al., 1993; Najman, 2006; Parkash et al., 1980]. Due to continued convergence of Indian plate, this Sub–Himalayan sequence was severely folded and thrusted during the late Holocene, and the continued underthrusting of the Indian plate under the Himalayas resulted in the development and activation of HFT [Mugnier et al., 1999; Sinha et al., 1987; Valdiya, 1988]. The HFT demarcates the tectonic/physiographic boundary between the southern margin of the Sub–Himalayan sequence and the recent Indo–Gangetic Plains (IGP, also known as alluvial plains) [Gansser, 1981; Jayangondaperumal et al., 2018; Nakata et al., 1991; Sinha et al., 1987; Thakur et al., 2019; Valdiya, 1988].

The Lesser Himalaya: structurally emplaced over the Sub–Himalaya, delimited by the MBT to the south and MCT to the north, this zone is primarily comprised of Middle Proterozoic to Mesozoic non–metamorphic to lower metamorphic–grade sedimentary rocks, deposited on the

Indian continental margin, belongs to the southernmost facies of the Tethyan Sea, and thrusted granitic and gneissic rocks of Indian continental crust [Celerier et al. 2009; DeCelles et al., 2004; Hodges, 2000; Martin, 2017; Parrish and Hodges, 1996; Robinson et al., 2006; Srivastava and Mitra 1994; Thakur et al., 2019; Upreti, 1999; Valdiya, 1980], and Paleogene sedimentary rocks of foreland basin [Srikantia and Bhargava, 1967; Srikantia and Sharma, 1970; Sakai, 1989; DeCelles et al., 1998a; Najman and Garzanti, 2000]. This sequence underwent considerable neotectonic activity during the mid–late Miocene [Valdiya, 1988; DeCelles et al., 2001; Robinson et al., 2006], maybe with some recent motion as young as Pliocene–Quaternary [Mugnier et al., 1994; Meigs et al., 1995; Mukherjee et al., 2015] in a form of foreland–propagating fold and thrust belt sequence due to differential movements along the MBT. Additionally, the Precambrian–Cambrian autochthonous bodies are exposed within the tectonic windows in the Lesser Himalaya, stretching west to east from the Himachal to the western Nepal Himalaya. Examples of these tectonic windows are the Almora nappe, the Ramgarh nappe, and the Krol nappe. The Almora nappe is a result of the tectonic transfer of rocks from the Higher Himalayan Metamorphic Belt to the Lesser Himalaya by the MCT during Eocene–Oligocene [Ahmad et al., 2000; DeCelles et al., 2001]. The largest Klippe/nappe distributed along the Himalayan arc is the Almora nappe [Mandal et al., 2015]. The northern and southern flanks of the Almora nappes are referred as the North Almora Thrust (NAT) and the South Almora Thrust (SAT) respectively [Heim and Gansser, 1939; Gansser, 1981]. The northern limb is thinner and steeply inclined (45°–75°, SSW/SW direction) whereas the southern limb is thicker and gently dipping (20°–30°, NNE/NE direction) [Valdiya and Kotlia, 2001]. The presence of the mylonitic sequence is another factor that distinguishes a large–scale shear zone of the NAT [Joshi et al., 2016; Joshi and Tiwari, 2009]. Ramgarh Thrust (RGT) is one of the main fault systems of the Himalayan fold and thrust belt in Uttarakhand and the western Nepal Himalayas. The RGT is about 0.2 to 2 km thick sheet may be traced running parallel to the strike of the Himalaya over its entire length in the Uttarakhand and western Nepal. The fault generally places the younger Lesser Himalayan rocks or lower Miocene foreland basin deposits over the oldest Paleoproterozoic rocks in the Lesser Himalayan group [Pearson and DeCelles, 2005].

The Greater Himalaya (or Higher Himalaya): structurally emplaced over the Lesser Himalaya, delimited by the MCT to the south and the STDS to the north, this zone also known as the core of the Himalayan Range, this zone is primarily comprised of the Indian continental crust, meta–sedimentary and meta–igneous rocks of Proterozoic–Ordovician age, regionally metamorphosed and deformed at mid-crustal depths during Oligocene–early Miocene, and intruded by crustal melts of leucogranite during early Miocene in the uppermost part [Parrish and Hodges, 1996; Deniel et al., 1987; Le Fort et al., 1987; Sinha, 1987; Guillot and Le Fort, 1995; Guillot et al., 1994, 2008; de Sigoyer et al., 2000; Treloar and Searle, 1993; Scaillet et al., 1995; Searle, 1999; Upreti, 1999; Ahmad et al., 2000; Najman and Garzanti, 2000; Godin et al., 2001; Searle and Treloar, 2019; Larson et al., 2010; Streule et al., 2010; Thakur et al., 2019]. The movement along the MCT that carried a hot slab of Higher Himalayan rocks over the cold Lesser Himalayan sequence is typically responsible for the well-known inverted metamorphism of the Himalaya and the late orogenic magmatism [Harrison et al., 1998, 1999; Upreti, 1999; Yin and Harrison, 2000]. In the early Miocene (22–19 Ma), roughly synchronous with the MCT that lifted the Greater Himalayan sequence above the Lesser Himalayan sequence, the STDS was active between the Tethyan sedimentary sequence and the Greater Himalayan sequence. STDS is a north-dipping, top-to-the-north normal system of steeper brittle faults and low–angle ductile shear zones [Yin and Harrison, 2000; Yin, 2006; Godin and Harris, 2014].

The Tethyan Himalaya (or Tibetan Himalaya): structurally overlies the Greater Himalaya, delimited by the STDS to the south and the ITSZ to the north, this zone is primarily comprised of Tethyan sedimentary succession of Proterozoic to Eocene age, represents the fossiliferous shelf deposits on the northern Indian continental margin [Gansser, 1964; Gaetani and Garzanti, 1991; Hodges; 2000; Upreti, 1999; Najman and Garzanti, 2000; Murphy and Yin, 2003; Murphy and Copeland, 2005; Gao et al., 2016; Thakur et al., 2019] interbedded with mafic volcanic rocks [Yin, 2006]. The distal Indian continental margin is made up of mafic lavas and plutonic rocks of Permian, Triassic, lower Cretaceous, Eocene–Miocene, and Cambrian–Eocene age (Garzanti et al., 1987; Hodges, 2000; Martin, 2017). From the Cambro–Ordovician pre–rift stage to the ultimate Early Cretaceous breakup of Gondwana, it documents the evolution of the Palaeo–Tethys and Neo–Tethys seas [Garzanti, 1999]. Additionally, lower Palaeozoic rocks at some locations near the Himalayan peaks have regional metamorphic assemblages that are consistent with intermediate to lower amphibolite–facies conditions [Coleman, 1996; Hodges et al., 1996]. The Himalayan orogen's highest structural position, also referred to as the superstructure [Godin, et al. 2006, 2011], is currently occupied by the weakly metamorphosed Tethyan sedimentary sequence fold and thrust belt system [Ratschbacher et al., 1994; Godin, 2003]. With ophiolite obduction [Ahmad et al., 2008; Searle et al., 1997; H'ebert et al., 2012] and following early crustal thickening in the Oligocene, the Tethyan sedimentary series likely preserves the earliest Himalayan deformation [Godin et al., 1999; Godin et al., 2001; Godin and Harris, 2014]. The generally recognized geological/tectonic boundary between the rock of Indian and Asian affinities, the ITSZ separates the Tibetan Plateau to the north from the Tethyan Himalaya orogenic wedge to the south [Gansser, 1980; Yin and Harrison, 2000; Zhang et al., 2012; Yang et al., 2017, 2019], represents the zone of collision between the India and Eurasian plates and is connected to the pre–continental collision obduction of the Tethyan ophiolites onto the leading edge of the Indian continental margin during the Late Cretaceous (~70 Ma) [Searle et al., 1997; Ahmad et al., 2000; H'ebert et al., 2012].

The Trans–Himalaya*:* this zone is comprised of deep–water Indian continental rise sediments, Trans–Himalayan accretionary prism complexes, forearc basin sedimentary rocks, obducted Neo–Tethys ophiolites and ophiolitic mélange, island arc volcanic rocks, upper Cretaceous to Eocene calc–alkaline island arc magmatic rocks related to subduction and collision, and post–collision molassic sediments [Ahmad et al., 2008; Buckman et al., 2018; Honegger et al., 1982; Searle, 1986; Coulon et al., 1986; Reuber et al., 1987; Garzanti and Van Haver, 1988; Reuber, 1986, 1989; Robertson and Degnan, 1993, 1994; Sharma, 1998; Najman and Garzanti, 2000].

The regional Himalayan strike (NW–SE), in the NW Himalaya bends along the Kangra re–entrant, and a transverse dextral–slip fault Ropar Manali Fault (RPMF) on the western margin of the Delhi–Haridwar Ridge (DHR) demarcates the boundary between the NW Himalaya and the central Himalaya segments [Heténeyi et al., 2016; Thakur et al., 2019]. Geological and geophysical observations demonstrate that the structural and seismic segmentation of the Himalayas is governed by lateral variations in geological structure, convergence, shortening rate, pre-orogenic sedimentary thickness, crustal thickness, erosion rates, thermal/exhumation patterns, stratigraphy, tectonic deformation pattern/style, lateral ramps along the main thrust faults, geometry of the MHT, cross–structures (e.g., DHR), and movements along the transverse faults/lineaments (e.g., RPMF, MGDF etc.) [Arora et al., 2012; Bai et al., 2019; Bollinger et al., 2004; Célérier et al., 2009; DiPietro and Pogue, 2004; Eugster et al., 2018; Gahalaut and Kundu, 2012; Gao et al., 2016; Gill et al., 2021; Gillian et al., 2015; Godin and Harris, 2014; Herman et al., 2010; Hetényi et al., 2016; Hubbard et al., 2021; Koulakov et al., 2015; Mandal et al., 2023; Murphy et al., 2014; Pandey et al., 1999; Prasad et al., 2011; Robert et al. 2011; Stevens and Avouac, 2015; Thakur et al., 2019; Vance et al., 2003; Whipp et al., 2007; Wu et al., 1998; Yadav et al., 2019, 2021; Yin, 2006]. Valdiya [1976] was one of the first who put up the idea that pre-Himalayan heterogeneities in the underplated Indian basement may be the primary reason for these along-strike variations. According to Valdiya [1976], transverse structures identified in the Himalaya could be the continuations of ancient faults and Ridges beneath the IGP that were reactivated during the evolution of the Himalayan orogen. Dasgupta et al. [1987] speculated that some transverse lineaments connected to the transverse ridges beneath the Himalayan foredeep, might be seismically active. Three notable subsurface faults identified south of the Himalayan front are the Great Boundary Fault (GBF), the Moradabad Fault (MBF), and the Mahendragrh-Dehradun Fault (MGDF). Segmentation is most obvious in the Kangra Renetrant and Nahan Salient regions of the NW Sub-Himalayan accretionary wedge, where the structure actively accommodates differential tectonic convergence across the two blocks due to left-lateral strike-slip mechanism with a component of uplift associated to thrusting along the HFT [Gill et al., 2021]. Dey et al. [2016] suggested that about 40–60% of the entire Sub-Himalayan shortening is accommodated by the thrusting along the Jwalamukhi Thrust (JMT) and hence strain partitioning along the foot of the Himalayan accretionary wedge in the Kangra re-entrant region, due to the JMT and other thrust faults over the Holocene age.

3 Data Analysis and Methodology

3.1 Data Analysis

In this study, we have combined six arrival time datasets recorded by local and regional seismograph networks (temporary and permanent) installed in the study region (25-35°N and 74-84°E). The combined dataset consist of arrival times of earthquakes recorded by International Seismological Center (ISC: www.isc.ac.uk) permanent network (Magnitude 3 and above; Period: 1974-2021), National Centre for Seismology, Govt. of India (NCS: www.seismo.gov.in) permanent network (Magnitude 2 and above; Period: 1998-2021), Incorporated Research Institution for Seismology (IRIS: www.iris.edu; Roecker and Levin, 2007) temporarily deployed network Y2 (Magnitude 3 and above; Period: 2007-2011), Réseau Sismologique et géodésique Français (RESIF-SISMOB: www.ws.resif.fr; Bollinger et al., 2011) temporarily deployed network HiK-NET (Magnitude 2 and above; Period: 2014-2016), Wadia Institute of Himalayan Geology, Govt. of India (WIHG: www.wihg.res.in) permanent network WIHG-I (Magnitude 2 and above; Period: 2007-2020), and Wadia Institute of Himalayan Geology, Govt. of India (WIHG: www.wihg.res.in) permanent network WIHG-II (Magnitude 2 and above; Period: 2016-2020). The seismographs network coordinates are given in Table S1. The earthquakes recorded by WIHG-I and WIHG-II networks were routinely analyzed and located through SEISAN [Ottemöller et al., 2021]. While combining different datasets we followed the criteria for identification of common events with close origin times should be ≤ 8 s and geographic coordinates should be ≤ 20 km. Considering the importance of slightly out-of-network events, we incorporated the same, as they considerably increase the ray coverage especially for greater depths as suggested by Zhao et al. [2007] and Koulakov, [2009b]. At the same time, they provide positive effects on tomography and enhance the resolution of tomographic images on the outer edges of the study area especially for greater depths.

After combining the dataset, we relocated the earthquakes using 1-D reference velocity model through LOTOS algorithm [Koulakov, 2009a]. The details about the computation of 1-D reference velocity model will be discussed in the next section. After relocation, the combined initial dataset consists of 1,36,125 picks with the corresponding P – and S – phases from 12,395 events recorded at 178 seismographs installed in the study region. For tomographic analysis we followed a 3 steps main criterion for earthquake events to be included in inversion process:

(i) number of rays per event should be ≥ 8;

(ii) the residuals for P – and S – rays after initial location of sources in 1-D reference velocity model should be < 1.5 and 2 s, respectively;

(iii) distance from an event to the nearest recording station should be ≤ 250 km.

After applying the selection criteria part of the data were filtered out, and the final dataset qualify for an iterative source location and tomographic analysis, consist of 99,048 picks with the corresponding 52,702 P - wave rays and 46,346 S – wave rays from 7,177 events (on an average 14 rays/event but not < 8) recorded at 178 seismic stations installed in the study region. The distribution of earthquakes and recording stations selected for computations is shown in Figure 2. The distribution of earthquake sources and receivers in the study area especially along the tectonic trend of the Himalayan Arc is good and quite homogenous (Figure 2) that ensures the high resolution of the tomographic inversions. In addition, to corroborate we have obtained the gravity data as Free-Air gravity anomaly (FAGA) and spherical Bouguer gravity anomaly (BGA) grids (WGM2012) [Bouvalot et al., 2012] from the International Gravimetric Bureau (BGI: www.bgi.obs-mip.fr), and topography data from ETOPO_2022 digital elevation model (15-arc second global relief model) of the earth's surface that integrates the land topography and the ocean bathymetry [Amante and Eakins, 2009], available at the National Geophysical Data Centre (NGDC: www.ngdc.noaa.gov).

Figure 2: Map showing the distribution of relocated seismicity in the final 3-D velocity model after 3 iterations (blue dots). Red triangles show seismic stations involved in this study. Green lines with numbers show six profiles selected for visualization of the main results in cross-sections, taken along as well as across the tectonic trend of the collision zone. Background topography is shown.

3.2 3-D Tomographic Inversion

The results of the 3-D seismic tomographic inversion are highly dependent on the quality of data and preliminary 1-D reference velocity models used for the inversion [Kissling et al., 1994]. We tried a number of 1-D velocity models as initial models and carried out 3-D inversion. Here, our objective is to study the varying nature and configuration of the Moho and the lithospheric mantle. We do not look for small scale crust/mantle heterogeneities. Therefore, here we do not predefine Moho depth and the corresponding velocity at Moho depth. In other words, here we do not parameterize the Moho as a sharp first-order interface. Instead, we set the reference 1-D velocity model without any high velocity gradients and even without any sharp interfaces. We determine geometry of Moho boundary by considering velocity anomalies. The velocity around the Moho depths in the preliminary 1-D reference velocity model will be faster than expected crustal velocities but slower than that of mantle velocities. As a result, the crust will be identified as a low-velocity anomaly body, whereas the uppermost mantle as a high-velocity anomaly body. Thus, variations in low-velocity anomaly may represents variations in crustal thickness or disturbances in Moho boundary geometry. We define 1-D reference velocity model with constant Vp/Vs ratio equals to 1.75 and set the P – wave velocity (Vp) at different depths as: 5.60 km/s at -5 km depth, 6.25 km/s at 25 km depth, 7.4 km/s at 40 km depth, 7.8 km/s at 65 km depth, 8.00 km/s at 120 km depth, 8.10 km/s at 165 km depth, and 8.20 km/s at 210 km depth. S – wave velocities were computed simply by diving the Vp by 1.75. The preliminary 1-D reference velocity models used for 3-D inversion are shown in Figure 3, and Table S2. During the inversion process the velocity is linearly interpolated between the defined depth levels.

Figure 3: Preliminary 1-D Reference Velocity Models. Red and blue lines indicate P – wave and S – wave velocity respectively.

3-D tomographic inversion was performed using LOTOS algorithm [Koulakov, 2009a; Koulakov et al., 2010] and this efficient algorithm has been implemented in many tomographic studies conducted in the Indo-Asia collision zone [e.g., Koulakov et al., 2015; Medved et al., 2022; Mukhopadhyay et al., 2014, 2016; Raoof et al., 2017, 2018, 2019; Sychev et al., 2018], as well as in different regions of the world [e.g., D'Auria et al., 2022; Garcia et al, 2019; Estève et al., 2022; Kasatkina et al., 2022; Koulakov et al., 2010; Singh et al., 2019; Talebi et al., 2020; Yaroshenko et al., 2022] and demonstrated new findings.

This algorithm uses local and regional earthquake data to conduct an iterative simultaneous inversion of body wave arrival times (P – and S – wave) and source coordinates. The result comes in the form of 3-D distribution of P – and S – wave velocities and relocated source coordinates in the 3-D velocity model.

The tomographic inversion was performed in four major steps: (1) computation of a reference traveltimes table using preliminary 1-D reference velocity model, where this stage involves computing the traveltimes for all feasible combinations of hypocentral depths and epicentral distances for earthquake sources using analytical formulae [Nolet, 1981]; (2) using a reference traveltimes table calculated in step (1), determining the sources' approximate locations based on the grid search approach [Koulakov and Sobolev, 2006]; locating the sources in the 3-D velocity model (in the first iteration, the initial 1-D reference velocity model is utilized, and in the succeeding iterations, the updated 3-D velocity models are used); (4) and velocity model inversion using multiple parameterization grids. The steps (3) and (4) are iterated over a number of times, one after the other. The bending method was utilized for 3-D ray tracing which is based on the successive modification of the ray path to achieve the shortest possible travel time [Koulakov, 2009a]. The idea of 3-D bending for ray tracing was first proposed by Um and Thurber [1987]. The effects of topography on 3-D tomographic inversions have been taken into account by taking into consideration the elevation of the seismograph stations. The earthquake sources are permitted to be located below the topographic surface. This efficient algorithm takes into account for the spherical nature of the Earth. Even though the computations are performed in Cartesian coordinates, the reference model is defined as a radially symmetric spherical model [Koulakov et al., 2010, 2015]. The parameterization of the velocity model was carried out by an algorithm proposed by Koulakov et al. [2006] using a grid of nodes allocated in the study volume in accordance with the ray density. In the horizontal direction the nodes were allocated with regular spacing of 20 km (in present case) in the areas of sufficient ray density (10 % of the average ray density) only. In the vertical direction the nodes were allocated with the spacing of 5 km (in present case), where the spacing inversely depends on the ray density and cannot be smaller than 5 km. As lowest resolvable size of the velocity anomalies is smaller than that of the defined grid spacing, therefore every pattern in the model is based on many nodes. This lessens the effect of the grid geometry on the outcome. The inversion was carried out by employing four grids with different fundamental orientations (0°, 22°, 45°, and 67°) independently, and the results were then stacked into one model to lessen the influence of node distributions in the results. The estimated model served as an updated 3-D velocity model in the following cycle of iterations. An iterative Least Square with QR factorization (LSQR) algorithm [Paige and Saunders, 1982; van der Sluis and van der Vorst, 1987], probably the most popular of the iterative algorithms in tomography problems, was used to invert the entire sparse matrix for simultaneous determination of velocities (Vp, Vs), and hypocentral parameters (dx, dy, dz, and dt) with respect to the reference 1-D velocity model. We have used only three cycles of iterations for both real and synthetic data inversions (a compromise between the quality of the solution and the computation time). To stabilize the solution, we employed the two types of regularization co-efficient: amplitude damping and smoothening/flattening co-efficient (minimizing the differences in the velocity at neighboring nodes). Several synthetic tests were conducted to evaluate the optimum values of the regularization parameters that enable for the optimum recovery of the recognized synthetic structures. The Tikhonov regularization, which presumes introducing a set of trivial equations for all grid nodes, was used for damping the amplitudes of the anomalies. We used the co-efficient of amplitude damping as (0.7) for P – and (1.2) for S – models. Another regularization co-efficient, smoothening/flattening co-efficient that smoothens the resulting model in the horizontal as well as vertical directions. We used the values for co-efficient of smoothening as (2.0) for P – and (3.0) for S – models. Synthetic modeling was also used to evaluate the weights for the station corrections. We used the values for weights for the station corrections as (0.45) for P – and (0.45) for S – models. After that, computations based on the real data were performed using the same set of regularization co-efficient and weights for station corrections.

In total we have performed five iterations, but consider only three iterations as the best for showing the main results. Table S3 shows the values of the mean residuals and the variance reductions for the P – and S – wave data. It should be emphasized that we have provided the mean residuals values in L1 norm. The mean residual deviations in the L1 norm decreased from 0.7663162 to 0.6021442 s (21.42354 %) for the P – wave data and from 1.30105 to 0.9028781 s (30.60389 %) for the S – wave data after three cycles of inversions and the subsequent relocation of the earthquake sources.

4 Results and Discussion

4.1 Synthetic Modelling

In this study we have performed tomographic inversion for 3-D distributions of P – wave (Vp) and S – wave (Vs) velocities and earthquake source locations. Our prime aim is to reconstruct the configuration of Moho depth and geometry of the subducting/underthrusting lithospheric mantle. As, we know that S – wave is very sensitive to fluids, cracks/fractures and temperature and pressure variations. Therefore, we cannot rely that much on the geometry reconstructed through Vs anomalies as compared to Vp anomalies. We may misinterpret the geometry of the reconstructed velocity structures through Vs anomalies. Thus herein, we only exhibit results for Vp anomalies. We exhibit here the outcomes of the synthetic modeling to evaluate the robustness and reliability of the acquired tomographic results before presenting the major results with 3-D distributions of the P – wave velocity (Vp) anomalies. In addition to assess the spatial resolution of the recovered velocity models, synthetic tests can aid in determining the optimal values of free inversion parameters (weights for source parameters and station corrections, smoothening / flattening co-efficient, amplitude damping co-efficient, number of iterations, etc.), as well as in estimating the actual amplitudes of the recovered velocity anomalies. The synthetic modelling is carried out in a way which is as closely as possible to how real data processing is carried out. The same 3-D bending algorithm is used for ray tracing to determine the travel times for the same sources and receivers' locations as in the real data inversion scenario. Then, to achieve approximately the same variance reduction as that of real data inversion, random noise with an average deviation of 0.1 s (in present case) is used to perturb the computed synthetic travel times. Then, using the same algorithm used for real data inversion, we completed the full data processing, including the steps for source locations, after computing the synthetic travel times and "forgot" all the information containing the velocity distributions and source locations. To examine the horizontal and vertical resolutions with the given data set, we conducted a number of synthetic tests (synthetic test using realistic pattern or free-shape anomalies (e.g., variable Moho depth model and subducting/underthrusting lithospheric slabs in this case), vertical checkerboard test, and horizontal checkerboard test.

Synthetic Test through Free-Shape anomalies

The outcome of the free-shape anomalies, which was used to evaluate the horizontal and vertical resolution of the recovered variable Moho depth model and geometry of the subducting/underthrusting lithospheric slabs, is shown in Figure 4. This test demonstrates the algorithm's capacity and efficiency to resolve the realistic velocity structures with the present data set. The synthetically recovered outcomes (Figure 4) show that we have enough resolution to distinguish and demonstrate the recovered model in the real data inversion scenario. Here, we define the synthetic models within the distance limits of ± 30 km across the profile with an amplitude of ± 10 %. In Figure 4, we show the results for two models as described above. In this case, the modelled anomalies don't change with depth. We can observe that the shapes and amplitudes have been correctly reconstructed. This test demonstrates the viability of a robust reconstruction of the geometry of the Moho boundary as well as the geometry of the subducting/underthrusting lithospheric slabs.

Figure 4: Synthetic tests to assess the vertical resolution in cross-sections along the profiles 2 and 5. The configuration of the synthetic anomalies defined as that of realistic anomalies. Positions of the profiles are shown in map view. (a) Synthetic test with reconstruction of the "variable Moho" depth model in relative P – wave velocity (Vp) anomalies along section 2 and 5. Black line highlight the configuration of Synthetic Moho. (b) Synthetic test with realistic configuration of the anomalies representing subducting/underthrusting lithospheric slabs, as observed in section 5. Top low-velocity anomaly is demarcated as Moho boundary with varying configuration from west to east in section 2 and south to north in section 5, and bottom high-velocity anomalies demarcated are subducting/underthrusting Indian mantle lithosphere towards north and subducted Tibetan slab towards south. We show the synthetic model (bottom) and recovered results (top) for the P – wave velocity (Vp) model.

Vertical Checkerboard Test

In comparison to the horizontal resolution, the vertical resolution is usually poor in local and regional passive source tomographic studies. The severity of this issue increases for broader areas, when the rays' depth of penetration is substantially lower than their length. Nearly horizontal rays are unable to reliably determine the change in velocity with depth in this situation. Figure 5 shows the outcomes of synthetic modelling through vertical checkerboard test. In this test checkerboard anomalies are defined along each of the six profiles utilized for presenting the main results. On each of the profiles the checkerboard anomalies are defined with 80 × 80 km size in horizontal direction and 60 km in vertical direction with an amplitude of ± 10 %. It can be clearly identified that the anomalies change the signs, at depths of 60 km, 120 km, etc. The recovered results (Figure 5) clearly demonstrate that the velocity model has good resolution for the two upper layers (60 and 120 km depths) along all the sections. Whereas, along sections 4 and 5 we can see some alternation of anomalies that changes their signs at deeper levels beneath the Indo-Asia collision boundary and southwest Tibet. This is due the presence of Y2 network and occurrence of mantle earthquakes as reported by many researchers [e.g., Chen and Yang, 2004; Feldl and Bilham, 2006; Liang et al., 2008; Nabelek et al., 2009; Xu et al., 2017; Wu et al., 1998; Priestley et al., 2008]. Therefore, we consider that our reconstructed velocity models have good resolution up to ~120 km and ~150 km depths beneath the Himalayas and the Indo-Asia collision boundary and southwest Tibet respectively.

Figure 5: Results of checkerboard test to assess the vertical resolution of P – wave velocity (Vp) model along the six profiles selected for presenting the main results. Thin black lines highlight the shapes of initial synthetic patterns. The size of the initial input synthetic model is 80×80×60 km. The locations of the profiles are shown in map view.

Horizontal Checkerboard Test

In this test, the initial synthetic model has alternating anomalies with sizes of 80 × 80 km with separation of 10 km, and amplitudes of ±10 % that are constant at all depths. At depths as low as 80 km, we can see that the primary patterns are correctly resolved. In the center of the region, where the majority of seismic stations are located, the best resolution is achieved. The anomalies are diagonally smeared outside the station network, yet at the right places, the alternation of anomalies may still be seen. Figure S1 shows the outcomes of synthetic modelling through horizontal checkerboard test conducted for assessing the horizontal resolution of the recovered velocity model.

4.2 Real Data Inversion Results

The estimated tomographic images of Vp – anomalies through real data inversion, are presented as horizontal slices (figure 6) for six depth levels (30 km, 35 km, 40 km, 50 km, 60 km, and 70 km), and cross-sections taken along the six selected profiles (Figure 7). The profiles are selected in a way that three profiles (1, 2 and 3) are along the tectonic trend of the Himalayas and three profiles (4, 5 and 6) are across the tectonic trend of the Himalayan–Tibetan orogen, more or less perpendicular to the strike of the Himalayas. Where, profiles 1, 2 and 3 are selected intentionally in a way that pass through the well-defined litho-tectonic subdivisions of the Himalayas; the Sub-Himalaya, the Lesser Himalaya and the Greater Himalaya respectively (Figures 2 and 6). The estimated tomographic images are well consistent and in good agreement with the overall geotectonic structure of the study region. Major geological structures are clearly discerned in the estimated tomographic images. The observed consistency in the Vp – anomalies relative to the geotectonic structure of the study region can be considered as evidence for the robustness of our results. Low Vp – anomalies represent the sediments/sedimentary rocks and high Vp – anomalies represent the high-density rigid material (Figures 6 and 7). Prominent low Vp – anomalies all along the Himalayan–Tibetan orogen may represents the sedimentary wedge/underthrusted crustal material below the Himalayas whereas high Vp – anomalies represent the high-density and rigid crustal material at shallower depths and Indian lithospheric mantle at deeper depths (Figure 6). The estimated tomographic images represented here as horizontal slices clearly demonstrate that low Vp – anomalies distributed all over the Himalayas and the southern Tibet at all depths except at 60-70 km depth below the Sub-Himalaya and Lesser Himalaya (Figure 6), represents the thicker crust containing sedimentary wedge and underthrusted crustal part of the Indian plate under the Himalayan-Tibetan orogen, as postulated by many researchers [Srivastava and Mitra, 1994; Hodges, 2000; Yin, 2006]. Low gravity anomaly, as well as isostatic model, supports the crustal thickening in the Himalayan-Tibetan orogen [Verma and Mukhopadhyay, 1977; Bonvalot et al., 2012]. However, the crust is relatively thinner below the Sub-Himalaya and the Lesser Himalaya as compared to the southern Tibet, where the crust seems to be greater than 70 km. This may be attributed to deeper roots/thicker crust developed by underthrusting of the Indian plate under the Eurasian plate. Prominent high Vp – anomaly at 30-35 km depths near the Delhi-Haridwar Ridge (DHR) area represents high-density and rigid crystalline material which is attributed to the hard and rigid rocks of the Precambrian age Delhi-Haridwar Ridge (DHR), a part of the Aravalli and Delhi fold belts running almost perpendicular to the tectonic trend of the Himalayas [Prasad et al., 2011; Qureshy, 1998; Rao et al., 2000]. It seems that this high Vp – body might be underthrusting the Himalaya, as speculated by many researchers [Gahalaut and Kundu, 2012; Hubbard et al., 2021]. The prominent low Vp – anomaly seems to be almost perpendicular to the strike of the Himalayas at a depth range of 40–50 km, may represents relatively thicker crust below the DHR as compared to the Himalayan foreland basin (Indo-Gangetic Plain).

Figure 6: Map view of tomographic images of P – wave velocity (Vp) anomalies for six selected depth levels (30, 35, 40, 50, 60 and 70 km depth) are presented. Black dots and cyan triangles show relocated seismicity in final 3-D velocity model and seismic stations involved respectively. Black lines demarcate major tectonic features (abbreviations are given in Figure 1).

Cross-sections of Vp – anomalies clearly demonstrate the crust and uppermost mantle structures beneath the study region (Figure 7). Exaggerated topography and regional Bouguer gravity anomaly (BGA) are shown on top and bottom of all the sections in respective segments (Figure 7) respectively. The observations of the Vp – anomalies are consistent all along the sections for the respective geotectonic units. We trace the lowest boundary of the low-velocity anomaly that may represents the crust-mantle boundary (Moho) along all the sections. We here report an undulating geometry of the Moho along the tectonic trend of the Himalayas (Figure 7). We note here that crustal thickness is lowest in the Himalayan foreland basin and start increasing gradually from below the Sub-Himalaya to the Higher Himalaya and reaches maxima below the southern Tibet. Section 4 (Figure 7) and Figure 9 show the effect of Delhi Haridwar Ridge (DHR) on the crustal part of the Himalayas. It shows that the crust here is buckled up. We propose that the ridge behaves like a beam that rams into the mountain chain, leading to such a buckling effect. Delhi-Haridwar ridge (DHR) is butting against the Himalayas (section 4, Figure 7). It is observed that the ridge seems to be underthrust the sub-Himalayas. This is the first time its northernmost extent is reported.

The gravity anomalies are related to the anomalous density and mass distributions within the Earth and thus shed light on the internal structure and composition of the Earth and play an important role in the lithospheric studies. The gravity anomalies serve as the most sensitive indicator of the degree and the way in which the topographic elements on the surface of the earth are compensated at depth [Karner and Watts, 1983]. The positive-negative gravity anomaly couple can be characterized as the static models of the density and mass distribution in the mountain ranges and their surroundings [e.g., Burov et al., 1990, 1998; Lin and Watts, 2002; Jordan and Watts, 2005; Kaban et al., 2010]. The positive gravity anomalies may represent the high-density rigid rocks within the crust and/or thin crust, whereas the flanking negative gravity anomalies may represent the over-thickened crust comprising of low-density crustal roots with sedimentary wedge [e.g., Watts and Daly, 1981; Bassett and Watts, 2015]. Large wavelength and short wavelength Bouguer gravity anomalies can be interpreted due to crustal thickening and folding/bulging or mid-crustal density heterogeneities respectively [Watts and Daly, 1981; Caporali, 2000]. The magnitude and wavelength of the Bouguer gravity anomaly are subject to the wavelength and elevation of the topography and the flexibility of the lithosphere, respectively [Karner and Watts, 1983]. Here in, the BGA and topography shows obvious corroboration with the density and/or mass distributions within the Himalayan-Tibetan orogen (Figure 7).

Figure 7: Cross-sections of P – wave velocity (Vp) anomalies along six selected profiles for the main results are presented. Positions of the profiles are shown with green lines and indicating numbers in map view of Vp anomalies at 45 km depth slice, where black dots and cyan triangles show distribution of relocated seismicity and seismic stations involved respectively, white lines demarcate major tectonic features (abbreviations are given in Figure 1). Exaggerated topography and Bouguer Gravity Anomaly (BGA) [after Bonvalot et al., 2012] are presented on top and bottom of cross-sections, along each profile. Arrows indicate major tectonic features where profiles intersect the same. Crust-Mantle boundary (Seismic Moho) is indicated with black lines in each of the cross-sections. Dotted black lines in section 5 indicate the underthrusting/subducting Indian Mantle Lithosphere towards north and subducted Tibetan Slab towards south. In cross-sections black dots indicate projections of relocated seismicity within 100 km on either side of the profiles.

We report here the regional variation in the thickness of the crust/lithosphere below the Himalayan-Tibetan orogen (Figure 7) that may be attributed to anomalous density/mass distributions. The observed undulations in the Moho geometry/crustal thickness and/or intra-crustal density/mass variations through our tomographic results are well corroborated with BGA and topography. Where, low/high BGA values are well corroborated with the negative/positive velocity anomalies respectively. Similar observations were made by Gao et al. [2003] in his study for the Baikal Rift zone as positive/negative travel time residuals in relation to low/high Bouguer gravity anomalies respectively. The highly negative Bouguer gravity anomalies over the Higher Himalayas and Tibet suggest the presence of thickened crust/lithosphere with relatively low-density roots with sedimentary wedge and underthrusted crustal fragments (Figure 7) beneath the Himalayan-Tibetan orogen. The observed local peaks of relatively high BGA values with respect to its general trend in the Lesser and Higher Himalayas are well corroborated with the over-thrusted high-density rigid crustal rocks associated with the MCT, MBT and other thrust faults movements in the Himalayas, as deciphered by high-velocity anomalies in the upper crust in my tomographic results (Figure 7). This suggests two possible scenarios: one that these bodies have relatively higher density as compared to the surrounding media, this is supported by my tomographic result; two that in these regions, isostatic compensation have not been achieved and hence resulted in the anomalous density/mass distributions that may represent variable crustal thicknesses. Therefore, the high-density rigid crystalline rocks of the upper crust most often coincide with the Himalayan seismic belt beneath the Himalayas as deciphered by the high-velocity anomalies in my tomographic image (Figure 7) suggests a hard and rigid crust with the excess density in the crust to subcrustal levels [Qureshy, 1971; Verma et al., 1976; Verma and Mukhopadhyay, 1977]. This could be due to the fact that these thrusted anomalous bodies are small enough or thrusted in fragments during the collision episodes, so that the lithosphere may hold them without buckling down substantially and hence the isostatic compensation may not have taken place. However, the BGA observed over IGP show BGA values having a flat spectrum with negative to near zero values at places where the estimated crusted thickness is ~40-45 km. This could be attributed due to the sediments resting over the hard basement and suggests that IGP region is relatively more or less in isostatic equilibrium as compared to the surroundings (Figure 7). The BGA values observed in the IGP region cannot be attributed to the sediment cover only, but can also be sought in terms of the crust and mantle relationships beneath the region and its root effect under the Himalayas [Qureshy, 1971; Verma et al., 1976] to the north where crustal thickness starts gradually increasing systematically from below the sub-Himalayas (40-50 km), below the Leser Himalayas (50-60 km), to below the Higher Himalayas (60-65 km), to below the Tethyan Himalaya (65-75 km) and reaches the deepest point below the southwest Tibet (75-85 km) after crossing ITSZ about ~300 km from the HFT (Figure 7). The gradient of negative BGA values is systematically increasing towards the Himalayan-Tibetan orogen to the north is a typical characteristic of the subduction/Collison zone.

Comparison with few published Moho depth estimates: In order to compare and produce the evidence of reliability of our recovered velocity models, we have also estimated the velocity models along the selected profiles taken from the recent published data [Gillian et al., 2015; Hazarika et al., 2021; Mandal, 2023; Mandal et al., 2023; Xu et al., 2017]. Figure 8 exhibits the reconstructed velocity models along the selected profiles. In figure 8, dotted line demarcates the Moho boundary estimated by different researchers through receiver function imaging technique. Thick black line demarcates the inferred Moho boundary through tomographic inversion of body wave arrival times in the present study. It is interesting to note that Moho boundary inferred with different datasets based on two different type of imaging techniques matches quite well. Hence, this also serves as another validation of our recovered velocity models. It should be emphasized here, that the inferred Moho boundary is shallowest beneath the Himalayan foreland basin and it starts gradually dipping from below the sub-Himalaya to the Higher Himalaya and reaches the deepest point below the southwest Tibet towards the north (Figure 8). We also report here that the crustal thickness also varies showing undulating configuration of Moho boundary along the tectonic trend of the Himalayas (Figure 8).

Figure 8: Cross-sections of P – wave velocity (Vp) anomalies along ten selected profiles taken from published literature are presented. Positions of the profiles are shown with white lines and indicating numbers in map view of Vp anomalies at 45 km depth slice, where black dots and cyan triangles show distribution of relocated seismicity and seismic stations involved respectively, White lines demarcate major tectonic features (abbreviations are given in Figure 1). Crust-Mantle boundary (Seismic Moho) is indicated with black lines in each of the cross-sections. Dotted black lines indicate the Moho along the same profile from published literature. In cross-sections black dots indicate projections of relocated seismicity within 100 km on either side of the profiles.

Moho depth map and Free-Air gravity anomaly (FAGA): To reconstruct the Moho depth map we have estimated the Vp – anomalies along the 48 profiles, 24 of them are along (Figure S2) and 24 are across (Figure S3) the tectonic trend of the Himalayas. To maintain the accuracy and reconstruct the more realistic and reliable configuration of Moho boundary we manually trace the bottom of the low-velocity anomaly at an interval of ~ 3-5 km along the well resolved portion of all the cross-sections. Figure S4 shows the positions of 48 selected profiles and Moho boundary picking points. We exhibit the reconstructed Moho depth map and regional free-Air gravity anomalies map in Figure 9. The Free-Air gravity anomalies (FAGA) exhibit quite large variations in the Himalayan-Tibetan orogen (Figure 9). Strong negative anomalies are seen to the south of the Himalayas, which may be a result of Indo-Gangetic alluvium carried from the Himalayas by extremely quick erosion as well as isostatic compensation associated to mountain building. The higher Himalayas bounded by MCT to the south and STDS to the north exhibits the strongest free-air gravity anomalies. It is obvious that the main cause of these extreme fluctuations in the FAGA along the Himalayan thrust zone is the abrupt Moho dipping from the Indian Plate's comparatively thin crust to the nearly doubled crust found beneath the Himalayas and Tibet. We also notice significant changes in gravity anomalies along the tectonic trend of the Himalayas, which may be attributed to the lateral inhomogeneity in the crustal thickness and or density/mass distributions. We also report that crustal thickness also varies below the Tibet from west to east, as evidenced by many researchers. Thus, our estimated Moho geometry through tomographic inversion is well corroborated with the observed regional gravity anomalies. For instance, the thinner crustal regions are associated with the lower FAGA values. On the other hand, thicker crust segments are linked to larger FAGA values.

Figure 9: (a) Estimated Moho depth beneath the study region in map view with epicenters of significant historical and recent large-magnitude earthquakes since 1501 CE. Red stars - epicenters of great earthquakes Mw ≥ 8; Blue stars - epicenters of major earthquakes with Mw 7–8; Black dots - epicenters of earthquakes with Mw 6–7; White dots – epicenters of earthquakes with Mw 5–6 (more details are given in Figure 1). Black lines demarcate major tectonic features (abbreviations are given in Figure 1). (b) Free-Air Gravity anomalies (FAGA) in map view derived from WGM 2012 [after Bonvalot et al., 2012]. White lines demarcate major tectonic features (abbreviations are given in Figure 1).

Variations of crustal thickness and their tectonic implications: We suggest a mechanism that could explain the variation in crustal thickness or undulating geometry of Moho boundary in the Himalayan-Tibetan orogen. The Indian plate's crust appears to be extremely heterogenous due to anomalous density/mass distributions and anomalous isostatic compensation. The existence of subducting basement Ridges (e.g., DHR) of Precambrian age comprising of crystalline rocks and ancient igneous provinces (crystalline basement beneath IGP) impacted by relict igneous processes may be one of the causes of substantial magmatic intrusions that may have significantly strengthened the Indian crust. However, thicker sediment piles and the sedimentary wedge material could account for the thicker crust and higher FAGA and lower BGA values. These two varieties of crust have different mechanical effects and behave differently during the episodes of Indo-Asia collision. The compression of the crust in the collision zone would have been more pronounced because the crust influenced by igneous processes is stronger. The presence of thicker crust near the contact area (75-85 km) where present collision zone lie along the ITSZ (Figure 9), can be explained by a stronger pushing impact of the Indian plate's more rigid crust. Thus, the thicker crust in front of the colliding Indian plate front along the collision boundary may indicate a wider shortening zone which has been reported by many researchers as discussed in the introduction. The segment of the abnormally thinner crust that lie below the sub-Himalaya may be explained by a lower crustal compression rate due to weaker incoming crust and lubricating effects of thicker sediments with a reduced colliding impact. We report here that the crust is relatively thicker below the IGP and sub-Himalaya in the Himachal Himalaya towards northwest as compared to Uttarakhand Himalaya. We infer that this variation is due to the E-W compression in response to oblique convergence of the Indian plate, as Indian plate subducts below Hindu Kush region. Many researchers reported the oblique convergence of the Indian plate and strain partitioning [e.g., Dey et al., 2016; Stevans and Avouac, 2015; Yadav et al., 2019] of the Himalayas towards northwest (Figures 1 and 9). Herein, we first explain the mechanism responsible this along strike variation of the crustal thickness/geometry of the Moho boundary. This could be because of the fact that after the continental part of the Indian plate collided with that of the Eurasian plate at its western end, it rotated counter-clockwise [Treloar and Coward, 1991]. This would have caused the significant stresses along the tectonic trend of the Himalayas increasing eastward leading to crumpling of the crust. This would have caused the variation of the crustal thickness along the tectonic trend of the Himalayas. We also interpret that the Indian plate collided in episodes during ages with the Eurasian plate with differential convergence rates [Dewey et al., 1988; Capitanio et al., 2010; van Hinsbergen et al., 2011; Jagoutz et al., 2015] that may result in differential shortening rates from west to east and hence this mechanism might have played an important role in controlling the anomalous crustal thinning/thickening. Along strike varying episodic convergence rates might have also played an important role in controlling the crustal scale thrusting along the Himalayan thrust zone and the tectono-metamorphic processes that resulted in anomalous density/mass distribution.

Figure 10: Schematic interpretation of the estimated tomographic image resulting from P – wave velocity (Vp) anomalies in section 5. Black line demarcates Main Himalayan Thrust (MHT) [after Gao et al., 2016]. Dashed white line separates seismically active brittle upper crust with that of relatively weaker and ductile lower crust. In cross-sections black dots indicate projections of relocated seismicity within 100 km on either side of the profile. Position of the profile is shown with green line and indicating number in map view of Vp anomalies at 45 km depth slice, where black dots and cyan triangles show distribution of relocated seismicity and seismic stations involved respectively, White lines demarcate major tectonic

features (abbreviations are given in Figure 1). Arrows indicate major tectonic features where profile intersects the same.

Geodynamic model of the Himalayan-Tibetan orogen: Based on the estimated tomographic image, herein, we exhibit a schematic preorientation of the Geodynamic model of the Himalayan-Tibetan orogen (Figure 10). Section 4 (Figure 7) shows that the Indian plate is gently underthrusting the Eurasian plate. Whereas, section 5 (Figure 7) and Figure exhibit that Indian plate is subducting/underthrusting the Eurasian plate with increasing dip towards east. Based on this observation we infer that the Indian plate is torn into pieces differing in its northern limits and angle of subduction/underthrusting. Where its westernmost end subducts/underthrusts below the Eurasian plate with a gentle dip crossing ITSZ and KKMF (section 4, Figure 7). Section 4 passes through the Kaurik-Chango Rift (KK-CGR) area. On the other hand, towards east Indian plate subducts/underthrust with a relatively greater angle near ITSZ, approximately 250 km distant from HFT. It is interesting to note that section 5 (Figure 7) and Figure 10 exhibit subduction zone of two slabs, where subducted Tibetan slab can also be seen dipping southward below the southwest Tibet. We speculate that the Indian plate has been torn off into several pieces, this phenomenon has also been reported by several researchers [e.g., Li and Song, 2018]. We infer that there is vertical tear in the Indian plate that might be related to either by differential convergence rates and or counter clock wise rotation of the Indian plate or rifting phenomenon. Figure 10 clearly exhibits that the upper crust below the Himalayas appears to be more rigid where most of the seismic activity takes place and the lower crust is ductile with partial melts at places, as evidenced by strong negative velocity anomaly and devoid of seismic activity. Presence of seismicity in the uppermost mantle below the collision zone suggests that uppermost mantle of the continental lithosphere is strong enough to sustain the elastic strain accumulation required for earthquakes. Thus, seismic activity in the upper crust as well as in the uppermost mantle represents the bimodal distribution of seismicity beneath the Himalayan-Tibetan orogen. We herein, presents the scenario of two subducting slabs, Indian plate towards north whereas the Tibetan slab subducted southward, with the Tibetan crust sandwiched between the two plates resulted in overthickening of the crust. In addition, the variable geometry of the Moho boundary along the tectonic trend of the Himalayan-Tibetan orogen may indicate that the Indian plate subducted/underthrusted beneath the Eurasian plate in a piecewise manner as a consequence of differential convergence rates, counter clockwise rotation of the Indian plate and episodic collision.

5 Conclusions

We have estimated 3-D seismic velocity structures of the crust and uppermost mantle beneath the Himalayan-Tibetan orogen through travel time tomography using local and regional earthquake data in order to get a more comprehensive tomographic image of the study region. Different segments of the study region were studied by several researchers using travel time tomography, surface wave analysis, and receiver function analysis. Our results exhibit a more comprehensive image of this tectonically very complicated region. Our results are well resolved up to ~120 km and ~150 km depths beneath the Himalayas and southwest Tibet respectively. Herein, we exhibit first time the effect of ramming of the Himalayas by the DHR through tomographic image. This ramming has also led to locally buckling up of the crust below the Himalayas. We present the scenario of two subducting slabs, Indian plate towards north whereas the Tibetan slab subducted southward, with the Tibetan crust sandwiched between the two plates resulted in overthickening of the crust. We interpret that the variable geometry of the Moho boundary along the tectonic trend of the Himalayan-Tibetan orogen may indicate that the Indian plate subducted/underthrusted beneath the Eurasian plate in a piecewise manner as a consequence of differential convergence rates, counter clockwise rotation of the Indian plate and episodic collision. Most of the seismicity is concentrated only in the brittle upper crust beneath the Himalayas, mainly within the main Himalayan Seismic belt between MBT and MCT within top ~15-25 km depth. Presence of seismicity in the uppermost mantle below the collision zone suggests that uppermost mantle of the continental lithosphere is strong enough to sustain the elastic strain accumulation required for earthquakes. Thus, seismic activity in the upper crust as well as in the uppermost mantle represents the bimodal distribution of seismicity beneath the Himalayan-Tibetan orogen. Average crustal thickness increases from south to north in the Himalayas. It is observed that this thickness also varies along the tectonic trend of the Himalayas. The comprehensive tomographic image, estimated in this study provides further insight into the Geodynamics of the whole study region that helps to understand the tectonic deformation and earthquakes generating mechanisms.

Acknowledgments

We do not have any type of conflict of interests with anyone. Most of the data set is freely available at the data repositories (ISC, IRIS, NCS and RESIF) except the data from WIHG seismograph networks. This data can be accessed through reasonable request and that would depend on the approval of the competent authority. We are thankful to the director, WIHG (Dr. Kalachand Sain) for allowing and providing necessary facilities for conducting this research. We are thankful to ISC, IRIS, NCS and RESIF-SISMOB for earthquake dataset, NGDC for topography data, and BGI for gravity data for allowing free online access to the data used in this study. A subset of the earthquake data set from WIHG-I and WIHG-II networks are sponsored by the MoES: Eartah System Sciences Organization, Ministry of Earth Sciences (ESSO), Govt. of India with project grant MoES/P.O.(Seismo)/1(373A)/2019) and WIHG, DST, Govt. of India, respectively. JR is thankful to Prof. Ivan Koulakov (Trofimuk Institute of Petroleum Geology and Geophysics, Russia) for providing free online access to LOTOS algorithm. JR is especially thankful to Dr. Laurent Bollinger (French Alternative Energies and Atomic Energy Commission, Bruyères-le-Châtel, France) for providing catalog data of HiK-Net network. JR is also thankful to Dr. Rouf Ahmad Shah (Scientist, WIHG) for providing access to his workstation at the time of urgent need. JR is also thankful to Mohd Shawez (PhD candidate, WIHG) for helping in georeferencing of few maps.

Open Research

Most of the datasets [ISC / DMN (1983-2021); ISC / NCS (1974-2021); IRIS - Y2 (2007-2011); HiK-NET (IRIS/RESIF) - ZO (2014-2016)] used in this study are freely available through International Seismological Centre (ISC), Seismological Facility for the Advancement of Geoscience (SAGE), National Centre for Seismology, Govt. of India (NCS). However, datasets [WIHG -I (2007-2020); WIHG -II (2016-2020)] from Wadia Institute of Himalayan Geology seismographs network (WIHG) can be accessed through reasonable request and that would depend on the approval of the competent authority. The gravity data is freely available at the International Gravimetric Bureau (BGI). The topography data is freely available at the National Geophysical Data Center (NGDC). The LOTOS code used in this study is freely available (https://www.ivan-art.com/science/LOTOS/). The processed and combined arrival time data produced through all the datasets will be uploaded as a supplementary file at the time of publication.

ISC/DMN and ISC/NCS: http://www.isc.ac.uk/iscbulletin/search/bulletin/

IRIS - Y2 (2007-2011): http://service.iris.edu/fdsnws/dataselect/1/

HiK-NET (IRIS/RESIF) - ZO (2014-2016): http://ws.resif.fr/fdsnws/dataselect/1/

NCS: https://seismo.gov.in/bulletins

Gravity data (BGI: FAGA and BGA): https://bgi.obs-mip.fr/data-products/grids-and-models/wgm2012-global-model/

Topography data (NGDC): https://www.ncei.noaa.gov/maps/grid-extract/

References

Ahmad, T., Tanaka, T., Sachan, H. K., Asahara, Y., Islam, R., & Khanna, P. P. (2008). Geochemical and isotopic constraints on the age and origin of the Nidar Ophiolitic Complex, Ladakh, India: Implications for the Neo-Tethyan subduction along the Indus suture zone. *Tectonophysics*, *451*(1), 206–224. https://doi.org/10.1016/j.tecto.2007.11.049

Ahmad, Talat, Harris, N., Bickle, M., Chapman, H., Bunbury, J., & Prince, C. (2000). Isotopic constraints on the structural relationships between the Lesser Himalayan Series and the High Himalayan Crystalline Series, Garhwal Himalaya. *GSA Bulletin*, *112*(3), 467–477. https://doi.org/10.1130/0016-7606(2000)112<467:ICOTSR>2.0.CO;2

Allégre, C. J., Courtillot, V., Tapponnier, P., Hirn, A., Mattauer, M., Coulon, C., et al. (1984). Structure and evolution of the Himalaya–Tibet orogenic belt. *Nature*, *307*(5946), 17–22. https://doi.org/10.1038/307017a0

Arora, B. R., Gahalaut, V. K., & Kumar, N. (2012). Structural control on along-strike variation in the seismicity of the northwest Himalaya. *Journal of Asian Earth Sciences*, *57*, 15–24. https://doi.org/10.1016/j.jseaes.2012.06.001

Avouac, J.-P. (2003). MOUNTAIN BUILDING, EROSION, AND THE SEISMIC CYCLE IN THE NEPAL HIMALAYA. In *Advances in Geophysics* (Vol. 46, pp. 1–80). Elsevier. https://doi.org/10.1016/S0065-2687(03)46001-9

Bai, L., Klemperer, S. L., Mori, J., Karplus, M. S., Ding, L., Liu, H., et al. (2019). Lateral variation of the Main Himalayan Thrust controls the rupture length of the 2015 Gorkha earthquake in Nepal. *Science Advances*, *5*(6), eaav0723. https://doi.org/10.1126/sciadv.aav0723

Bassett, D., & Watts, A. B. (2015). Gravity anomalies, crustal structure, and seismicity at subduction zones: 1. Seafloor roughness and subducting relief. *Geochemistry, Geophysics, Geosystems*, *16*(5), 1508–1540. https://doi.org/10.1002/2014GC005684

Bendick, R., & Bilham, R. (2001). How perfect is the Himalayan arc? *Geology*, *29*(9), 791–794. https://doi.org/10.1130/0091-7613(2001)029<0791:HPITHA>2.0.CO;2

Besse, J., Courtillot, V., Pozzi, J. P., Westphal, M., & Zhou, Y. X. (1984). Palaeomagnetic estimates of crustal shortening in the Himalayan thrusts and Zangbo suture. *Nature*, *311*(5987), 621–626. https://doi.org/10.1038/311621a0

Besse, Jean, & Courtillot, V. (1988). Paleogeographic maps of the continents bordering the Indian Ocean since the Early Jurassic. *Journal of Geophysical Research: Solid Earth*, *93*(B10), 11791–11808. https://doi.org/10.1029/JB093iB10p11791

Bian, W., Yang, T., Ma, Y., Jin, J., Gao, F., Zhang, S., et al. (2017). New Early Cretaceous palaeomagnetic and geochronological results from the far western Lhasa terrane: Contributions to the Lhasa-Qiangtang collision. *Scientific Reports*, *7*(1), 16216. https://doi.org/10.1038/s41598-017-16482-3

Bilham, R. (2019). Himalayan earthquakes: a review of historical seismicity and early 21st century slip potential. *Geological Society, London, Special Publications*, *483*(1), 423–482. https://doi.org/10.1144/SP483.16

Bilham, R., & Ambraseys, N. (2005a). Apparent Himalayan slip deficit from the summation of seismic moments for Himalayan earthquakes, 1500–2000. *Current Science*, *88*(10), 1658–1663. Retrieved from https://www.jstor.org/stable/24110492

Bilham, R., & Ambraseys, N. (2005b). Apparent Himalayan slip deficit from the summation of seismic moments for Himalayan earthquakes, 1500–2000. *Current Science*, *88*(10), 1658–1663. Retrieved from https://www.jstor.org/stable/24110492

Bilham, R., Larson, K., & Freymueller, J. (1997a). GPS measurements of present-day convergence across the Nepal Himalaya. *Nature*, *386*(6620), 61–64. https://doi.org/10.1038/386061a0

Bilham, R., Larson, K., & Freymueller, J. (1997b). GPS measurements of present-day convergence across the Nepal Himalaya. *Nature*, *386*(6620), 61–64. https://doi.org/10.1038/386061a0

Bilham, R., Blume, F., Bendick, R., & Gaur, V. K. (1998). Geodetic constraints on the translation and deformation of India: Implications for future great Himalayan earthquakes. *Current Science*, *74*(3), 213–229. Retrieved from https://www.jstor.org/stable/24100867

Bollinger, L., Avouac, J. P., Cattin, R., & Pandey, M. R. (2004). Stress buildup in the Himalaya. *Journal of Geophysical Research: Solid Earth*, *109*(B11). https://doi.org/10.1029/2003JB002911

Buckman, S., Aitchison, J. C., Nutman, A. P., Bennett, V. C., Saktura, W. M., Walsh, J. M. J., et al. (2018). The Spongtang Massif in Ladakh, NW Himalaya: An Early Cretaceous record of spontaneous, intra-oceanic subduction initiation in the Neotethys. *Gondwana Research*, *63*, 226–249. https://doi.org/10.1016/j.gr.2018.07.003

Bungum, H., Lindholm, C. D., & Mahajan, A. K. (2017). Earthquake recurrence in NW and central Himalaya. *Journal of Asian Earth Sciences*, *138*, 25–37. https://doi.org/10.1016/j.jseaes.2017.01.034

Burg, J. P., & Chen, G. M. (1984). Tectonics and structural zonation of southern Tibet, China. *Nature*, *311*(5983), 219–223. https://doi.org/10.1038/311219a0

Burg, J.-P., & Bouilhol, P. (2019). Timeline of the South Tibet – Himalayan belt: the geochronological record of subduction, collision, and underthrusting from zircon and monazite U–Pb ages. *Canadian Journal of Earth Sciences*, *56*(12), 1318–1332. https://doi.org/10.1139/cjes-2018-0174

Burov, E., Jaupart, C., & Mareschal, J. C. (1998). Large-scale crustal heterogeneities and lithospheric strength in cratons. *Earth and Planetary Science Letters*, *164*(1), 205–219. https://doi.org/10.1016/S0012-821X(98)00205-2

Burov, E. V., Kogan, M. G., Lyon-Caen, H., & Molnar, P. (1990). Gravity anomalies, the deep structure, and dynamic processes beneath the Tien Shan. *Earth and Planetary Science Letters*, *96*(3), 367–383. https://doi.org/10.1016/0012-821X(90)90013-N

Caldwell, W. B., Klemperer, S. L., Lawrence, J. F., Rai, S. S., & Ashish. (2013). Characterizing the Main Himalayan Thrust in the Garhwal Himalaya, India with receiver function CCP stacking. *Earth and Planetary Science Letters*, *367*, 15–27. https://doi.org/10.1016/j.epsl.2013.02.009

Cande, S. C., & Stegman, D. R. (2011). Indian and African plate motions driven by the push force of the Réunion plume head. *Nature*, *475*(7354), 47–52. https://doi.org/10.1038/nature10174

Capitanio, F. A., Morra, G., Goes, S., Weinberg, R. F., & Moresi, L. (2010). India–Asia convergence driven by the subduction of the Greater Indian continent. *Nature Geoscience*, *3*(2), 136–139. https://doi.org/10.1038/ngeo725

Capitanio, F. a., Replumaz, A., & Riel, N. (2015). Reconciling subduction dynamics during Tethys closure with large-scale Asian tectonics: Insights from numerical modeling. *Geochemistry, Geophysics, Geosystems*, *16*(3), 962–982. https://doi.org/10.1002/2014GC005660

Caporali, A. (2000). Buckling of the lithosphere in western Himalaya: Constraints from gravity and topography data. *Journal of Geophysical Research: Solid Earth*, *105*(B2), 3103–3113. https://doi.org/10.1029/1999JB900389

Célérier, J., Harrison, T. M., Webb, A. A. G., & Yin, A. (2009). The Kumaun and Garwhal Lesser Himalaya, India: Part 1. Structure and stratigraphy. *GSA Bulletin*, *121*(9–10), 1262–1280. https://doi.org/10.1130/B26344.1

Chemenda, A. I., Burg, J.-P., & Mattauer, M. (2000). Evolutionary model of the Himalaya–Tibet system: geopoem: based on new modelling, geological and geophysical data. *Earth and Planetary Science Letters*, *174*(3), 397–409. https://doi.org/10.1016/S0012-821X(99)00277-0

Chen, W.-P., & Yang, Z. (2004). Earthquakes Beneath the Himalayas and Tibet: Evidence for Strong Lithospheric Mantle. *Science*, *304*(5679), 1949–1952. https://doi.org/10.1126/science.1097324

Coleman, M. E. (1996). Orogen-parallel and orogen-perpendicular extension in the central Nepalese Himalayas. *GSA Bulletin*, *108*(12), 1594–1607. https://doi.org/10.1130/0016-7606(1996)108<1594:OPAOPE>2.3.CO;2

Copley, A., Avouac, J.-P., & Royer, J.-Y. (2010). India-Asia collision and the Cenozoic slowdown of the Indian plate: Implications for the forces driving plate motions. *Journal of Geophysical Research: Solid Earth*, *115*(B3). https://doi.org/10.1029/2009JB006634

Coulon, C., Maluski, H., Bollinger, C., & Wang, S. (1986). Mesozoic and cenozoic volcanic rocks from central and southern Tibet:39Ar-40Ar dating, petrological characteristics and geodynamical significance. *Earth and Planetary Science Letters*, *79*(3), 281–302. https://doi.org/10.1016/0012-821X(86)90186-X

Critelli, S., & Garzanti, E. (1994). Provenance of the Lower Tertiary Murree redbeds (Hazara-Kashmir Syntaxis, Pakistan) and initial rising of the Himalayas. *Sedimentary Geology*, *89*(3), 265–284. https://doi.org/10.1016/0037-0738(94)90097-3

Dasgupta, S., Mukhopadhyay, M., & Nandy, D. R. (1987). Active transverse features in the central portion of the Himalaya. *Tectonophysics*, *136*(3), 255–264. https://doi.org/10.1016/0040-1951(87)90028-X

D'Auria, L., Koulakov, I., Prudencio, J., Cabrera-Pérez, I., Ibáñez, J. M., Barrancos, J., et al. (2022). Rapid magma ascent beneath La Palma revealed by seismic tomography. *Scientific Reports*, *12*(1), 17654. https://doi.org/10.1038/s41598-022-21818-9

De Franco, R., Govers, R., & Wortel, R. (2008). Dynamics of continental collision: Influence of the plate contact. *Geophysical Journal International*, *174*(3), 1101–1120. https://doi.org/10.1111/j.1365-246X.2008.03857.x

DeCelles, P. G., Gehrels, G. E., Quade, J., Ojha, T. P., Kapp, P. A., & Upreti, B. N. (1998). Neogene foreland basin deposits, erosional unroofing, and the kinematic history of the Himalayan fold-thrust belt, western Nepal. *GSA Bulletin*, *110*(1), 2–21. https://doi.org/10.1130/0016-7606(1998)110<0002:NFBDEU>2.3.CO;2

DeCelles, P. G., Gehrels, G. E., Najman, Y., Martin, A. J., Carter, A., & Garzanti, E. (2004). Detrital geochronology and geochemistry of Cretaceous–Early Miocene strata of Nepal: implications for timing and diachroneity of initial Himalayan orogenesis. *Earth and Planetary Science Letters*, *227*(3), 313–330. https://doi.org/10.1016/j.epsl.2004.08.019

DeCelles, P. G., Carrapa, B., Gehrels, G. E., Chakraborty, T., & Ghosh, P. (2016). Along-strike continuity of structure, stratigraphy, and kinematic history in the Himalayan thrust belt: The view from Northeastern India. *Tectonics*, *35*(12), 2995–3027. https://doi.org/10.1002/2016TC004298

DeCelles, Peter G., Gehrels, G. E., Quade, J., & Ojha, T. P. (1998). Eocene-early Miocene foreland basin development and the history of Himalayan thrusting, western and central Nepal. *Tectonics*, *17*(5), 741–765. https://doi.org/10.1029/98TC02598

DeCelles, Peter G., Robinson, D. M., Quade, J., Ojha, T. P., Garzione, C. N., Copeland, P., & Upreti, B. N. (2001a). Stratigraphy, structure, and tectonic evolution of the Himalayan fold-thrust belt in western Nepal. *Tectonics*, *20*(4), 487–509. https://doi.org/10.1029/2000TC001226

DeCelles, Peter G., Robinson, D. M., Quade, J., Ojha, T. P., Garzione, C. N., Copeland, P., & Upreti, B. N. (2001b). Stratigraphy, structure, and tectonic evolution of the Himalayan fold-thrust belt in western Nepal. *Tectonics*, *20*(4), 487–509. https://doi.org/10.1029/2000TC001226

DeCelles, Peter G., Robinson, D. M., & Zandt, G. (2002). Implications of shortening in the Himalayan fold-thrust belt for uplift of the Tibetan Plateau. *Tectonics*, *21*(6), 12-1-12–25. https://doi.org/10.1029/2001TC001322

DeMets, C., Gordon, R. G., Argus, D. F., & Stein, S. (1994). Effect of recent revisions to the geomagnetic reversal time scale on estimates of current plate motions. *Geophysical Research Letters*, *21*(20), 2191–2194. https://doi.org/10.1029/94GL02118

DeMets, C., Gordon, R. G., & Argus, D. F. (2010). Geologically current plate motions. *Geophysical Journal International*, *181*(1), 1–80. https://doi.org/10.1111/j.1365-246X.2009.04491.x

Deniel, C., Vidal, P., Fernandez, A., Le Fort, P., & Peucat, J.-J. (1987). Isotopic study of the Manaslu granite (Himalaya, Nepal): inferences on the age and source of Himalayan leucogranites. *Contributions to Mineralogy and Petrology*, *96*(1), 78–92. https://doi.org/10.1007/BF00375529

Dewey, J.F., Cande, S., & Pitman III, W. C. (1989). Tectonic evolution of the India/Eurasia Collision Zone. *Eclogae Geologicae Helvetiae*, *82*(3), 717–734.

Dewey, John Frederick, Shackleton, R. M., Chengfa, C., Yiyin, S., Chengfa, C., Shackleton, R. M., et al. (1997). The tectonic evolution of the Tibetan Plateau. *Philosophical Transactions of the Royal Society of London. Series A, Mathematical and Physical Sciences*, *327*(1594), 379–413. https://doi.org/10.1098/rsta.1988.0135

Dey, S., Thiede, R. C., Schildgen, T. F., Wittmann, H., Bookhagen, B., Scherler, D., & Strecker, M. R. (2016). Holocene internal shortening within the northwest Sub-Himalaya: Out-of-sequence faulting of the Jwalamukhi Thrust, India. *Tectonics*, *35*(11), 2677–2697. https://doi.org/10.1002/2015TC004002

DiPietro, J. A., & Pogue, K. R. (2004). Tectonostratigraphic subdivisions of the Himalaya: A view from the west. *Tectonics*, *23*(5). https://doi.org/10.1029/2003TC001554

England, P., & McKenzie, D. (1982). A thin viscous sheet model for continental deformation. *Geophysical Journal International*, *70*(2), 295–321. https://doi.org/10.1111/j.1365-246X.1982.tb04969.x

Estève, C., Liu, Y., Koulakov, I., Schaeffer, A. J., & Audet, P. (2022). Seismic Evidence for a Weakened Thick Crust at the Beaufort Sea Continental Margin. *Geophysical Research Letters*, *49*(16), e2022GL100158. https://doi.org/10.1029/2022GL100158

Eugster, P., Thiede, R. C., Scherler, D., Stübner, K., Sobel, E. R., & Strecker, M. R. (2018). Segmentation of the Main Himalayan Thrust Revealed by Low-Temperature Thermochronometry in the Western Indian Himalaya. *Tectonics*, *37*(8), 2710–2726. https://doi.org/10.1029/2017TC004752

Feldl, N., & Bilham, R. (2006). Great Himalayan earthquakes and the Tibetan plateau. *Nature*, *444*(7116), 165–170. https://doi.org/10.1038/nature05199

Freymueller, J., Bilham, R., Bürgmann, R., Larson, K. M., Paul, J., Jade, S., & Gaur, V. (1996). Global Positioning System measurements of Indian Plate Motion and convergence across the lesser Himalaya. *Geophysical Research Letters*, *23*(22), 3107–3110. https://doi.org/10.1029/96GL02518

Gaetani, M., & Garzanti, E. (1991a). Multicyclic History of the Northern India Continental Margin (Northwestern Himalaya)1. *AAPG Bulletin*, *75*(9), 1427–1446. https://doi.org/10.1306/0C9B2957-1710-11D7-8645000102C1865D

Gaetani, M., & Garzanti, E. (1991b). Multicyclic History of the Northern India Continental Margin (Northwestern Himalaya)1. *AAPG Bulletin*, *75*(9), 1427–1446. https://doi.org/10.1306/0C9B2957-1710-11D7-8645000102C1865D

Gahalaut, V. K., & Kundu, B. (2012). Possible influence of subducting ridges on the Himalayan arc and on the ruptures of great and major Himalayan earthquakes. *Gondwana Research*, *21*(4), 1080–1088. https://doi.org/10.1016/j.gr.2011.07.021

Gansser, A. (1980). The significance of the Himalayan suture zone. *Tectonophysics*, *62*(1), 37–52. https://doi.org/10.1016/0040-1951(80)90134-1

Gansser, Augusto. (1981). The Geodynamic History of the Himalaya. In *Zagros Hindu Kush Himalaya Geodynamic Evolution* (pp. 111–121). American Geophysical Union (AGU). https://doi.org/10.1029/GD003p0111

Gao, R., Lu, Z., Klemperer, S. L., Wang, H., Dong, S., Li, W., & Li, H. (2016). Crustal-scale duplexing beneath the Yarlung Zangbo suture in the western Himalaya. *Nature Geoscience*, *9*(7), 555–560. https://doi.org/10.1038/ngeo2730

Gao, S. S., Liu, K. H., Davis, P. M., Slack, P. D., Zorin, Y. A., Mordvinova, V. V., & Kozhevnikov, V. M. (2003). Evidence for small-scale mantle convection in the upper mantle beneath the Baikal rift zone. *Journal of Geophysical Research: Solid Earth*, *108*(B4). https://doi.org/10.1029/2002JB002039

García, M. A., Vargas, C. A., & Koulakov, I. Y. (2019). Local Earthquake Tomography of the Nevado del Huila Volcanic Complex (Colombia): Magmatic and Tectonic Interactions in a Volcanic-Glacier Complex System. *Journal of Geophysical Research: Solid Earth*, *124*(2), 1688–1699. https://doi.org/10.1029/2018JB016324

Garzanti, E. (1999). Stratigraphy and sedimentary history of the Nepal Tethys Himalaya passive margin. *Journal of Asian Earth Sciences*, *17*(5), 805–827. https://doi.org/10.1016/S1367-9120(99)00017-6

Garzanti, Eduardo, & Van Haver, T. (1988). The indus clastics: forearc basin sedimentation in the Ladakh Himalaya (India). *Sedimentary Geology*, *59*(3), 237–249. https://doi.org/10.1016/0037-0738(88)90078-4

Garzanti, Eduardo, Baud, A., & Mascle, G. (1987). Sedimentary record of the northward flight of India and its collision with Eurasia (Ladakh Himalaya, India). *Geodinamica Acta*, *1*(4–5), 297–312. https://doi.org/10.1080/09853111.1987.11105147

Gill, H. S., Singh, T., Singh, S., Kim, J.-R., Caputo, R., Kaur, G., et al. (2021). Active transfer faulting in the NW Sub-Himalaya (India) observed by space-borne topographic analyses. *Quaternary International*, *585*, 15–26. https://doi.org/10.1016/j.quaint.2020.09.046

Gilligan, A., Priestley, K. F., Roecker, S. W., Levin, V., & Rai, S. S. (2015). The crustal structure of the western Himalayas and Tibet. *Journal of Geophysical Research: Solid Earth*, *120*(5), 3946–3964. https://doi.org/10.1002/2015JB011891

Godin, L., Grujic, D., Law, R. D., & Searle, M. P. (2006). Channel flow, ductile extrusion and exhumation in continental collision zones: an introduction. *Geological Society, London, Special Publications*, *268*(1), 1–23. https://doi.org/10.1144/GSL.SP.2006.268.01.01

Godin, Laurent. (2003). Structural evolution of the Tethyan sedimentary sequence in the Annapurna area, central Nepal Himalaya. *Journal of Asian Earth Sciences*, *22*(4), 307–328. https://doi.org/10.1016/S1367-9120(03)00066-X

Godin, Laurent, & Harris, L. B. (2014). Tracking basement cross-strike discontinuities in the Indian crust beneath the Himalayan orogen using gravity data – relationship to upper crustal faults. *Geophysical Journal International*, *198*(1), 198–215. https://doi.org/10.1093/gji/ggu131

Godin, Laurent, Brown, R. L., Hanmer, S., & Parrish, R. (1999). Back folds in the core of the Himalayan orogen: An alternative interpretation. *Geology*, *27*(2), 151–154. https://doi.org/10.1130/0091-7613(1999)027<0151:BFITCO>2.3.CO;2

Godin, Laurent, Parrish, R. R., Brown, R. L., & Hodges, K. V. (2001). Crustal thickening leading to exhumation of the Himalayan Metamorphic core of central Nepal: Insight from U-Pb Geochronology and 40Ar/39Ar Thermochronology. *Tectonics*, *20*(5), 729–747. https://doi.org/10.1029/2000TC001204

Godin, Laurent, Yakymchuk, C., & Harris, L. B. (2011). Himalayan hinterland-verging superstructure folds related to foreland-directed infrastructure ductile flow: Insights from centrifuge analogue modelling. *Journal of Structural Geology*, *33*(3), 329–342. https://doi.org/10.1016/j.jsg.2010.09.005

Guillot, S., & Le Fort, P. (1995). Geochemical constraints on the bimodal origin of High Himalayan leucogranites. *Lithos*, *35*(3), 221–234. https://doi.org/10.1016/0024-4937(94)00052-4

Guillot, S., Mahéo, G., de Sigoyer, J., Hattori, K. H., & Pêcher, A. (2008). Tethyan and Indian subduction viewed from the Himalayan high- to ultrahigh-pressure metamorphic rocks. *Tectonophysics*, *451*(1), 225–241. https://doi.org/10.1016/j.tecto.2007.11.059

Guillot, Stéphane, & Replumaz, A. (2013). Importance of continental subductions for the growth of the Tibetan plateau. *Bulletin de La Société Géologique de France*, *184*(3), 199–223. https://doi.org/10.2113/gssgfbull.184.3.199

Guillot, Stéphane, Hodges, K., Fort, P. L., & Pêcher, A. (1994). New constraints on the age of the Manaslu leucogranite: Evidence for episodic tectonic denudation in the central Himalayas. *Geology*, *22*(6), 559–562. https://doi.org/10.1130/0091-7613(1994)022<0559:NCOTAO>2.3.CO;2

Guillot, Stéphane, Garzanti, E., Baratoux, D., Marquer, D., Mahéo, G., & de Sigoyer, J. (2003). Reconstructing the total shortening history of the NW Himalaya. *Geochemistry, Geophysics, Geosystems*, *4*(7). https://doi.org/10.1029/2002GC000484

Harrison, T. M., Copeland, P., Hall, S. A., Quade, jay, Burner, S., Ojha, T. P., & Kidd, W. S. F. (1993). Isotopic Preservation of Himalayan/Tibetan Uplift, Denudation, and Climatic Histories of Two Molasse Deposits. *The Journal of Geology*, *101*(2), 157–175. Retrieved from https://www.jstor.org/stable/30081145

Harrison, T. M., Grove, M., Lovera, O. M., & Catlos, E. J. (1998). A model for the origin of Himalayan anatexis and inverted metamorphism. *Journal of Geophysical Research: Solid Earth*, *103*(B11), 27017–27032. https://doi.org/10.1029/98JB02468

Harrison, T. M., Grove, M., Lovera, O. M., Catlos, E. J., & D'Andrea, J. (1999). The origin of Himalayan anatexis and inverted metamorphism: Models and constraints. *Journal of Asian Earth Sciences*, *17*(5), 755–772. https://doi.org/10.1016/S1367-9120(99)00018-8

Hauck, M. L., Nelson, K. D., Brown, L. D., Zhao, W., & Ross, A. R. (1998). Crustal structure of the Himalayan orogen at ~90° east longitude from Project INDEPTH deep reflection profiles. *Tectonics*, *17*(4), 481–500. https://doi.org/10.1029/98TC01314

Hazarika, D., Hajra, S., Kundu, A., Bankhwal, M., Kumar, N., & Pant, C. C. (2021). Imaging the Moho and Main Himalayan Thrust beneath the Kumaon Himalaya: constraints from receiver function analysis. *Geophysical Journal International*, *224*(2), 858–870. https://doi.org/10.1093/gji/ggaa478

He, D., Webb, A. A. G., Larson, K. P., Martin, A. J., & Schmitt, A. K. (2015). Extrusion vs. duplexing models of Himalayan mountain building 3: duplexing dominates from the Oligocene to Present. *International Geology Review*, *57*(1), 1–27. https://doi.org/10.1080/00206814.2014.986669

He, D., Webb, A. A. G., Larson, K. P., & Schmitt, A. K. (2016). Extrusion vs. duplexing models of Himalayan mountain building 2: The South Tibet detachment at the Dadeldhura klippe. *Tectonophysics*, *667*, 87–107. https://doi.org/10.1016/j.tecto.2015.11.014

Hébert, R., Bezard, R., Guilmette, C., Dostal, J., Wang, C. S., & Liu, Z. F. (2012). The Indus–Yarlung Zangbo ophiolites from Nanga Parbat to Namche Barwa syntaxes, southern Tibet: First synthesis of petrology, geochemistry, and geochronology with incidences on geodynamic reconstructions of Neo-Tethys. *Gondwana Research*, *22*(2), 377–397. https://doi.org/10.1016/j.gr.2011.10.013

Herman, F., Copeland, P., Avouac, J.-P., Bollinger, L., Mahéo, G., Le Fort, P., et al. (2010). Exhumation, crustal deformation, and thermal structure of the Nepal Himalaya derived from the inversion of thermochronological and thermobarometric data and modeling of the topography. *Journal of Geophysical Research: Solid Earth*, *115*(B6). https://doi.org/10.1029/2008JB006126

Hetényi, G., Cattin, R., Berthet, T., Le Moigne, N., Chophel, J., Lechmann, S., et al. (2016). Segmentation of the Himalayas as revealed by arc-parallel gravity anomalies. *Scientific Reports*, *6*(1), 33866. https://doi.org/10.1038/srep33866

van der Hilst, R. D., Widiyantoro, S., & Engdahl, E. R. (1997). Evidence for deep mantle circulation from global tomography. *Nature*, *386*(6625), 578–584. https://doi.org/10.1038/386578a0

van Hinsbergen, D. J. J., Steinberger, B., Doubrovine, P. V., & Gassmöller, R. (2011). Acceleration and deceleration of India-Asia convergence since the Cretaceous: Roles of mantle plumes and continental collision. *Journal of Geophysical Research: Solid Earth*, *116*(B6). https://doi.org/10.1029/2010JB008051

Hodges, K. V. (2000). Tectonics of the Himalaya and southern Tibet from two perspectives. *GSA Bulletin*, *112*(3), 324–350. https://doi.org/10.1130/0016-7606(2000)112<324:TOTHAS>2.0.CO;2

Hodges, K. V., Parrish, R. R., & Searle, M. P. (1996). Tectonic evolution of the central Annapurna Range, Nepalese Himalayas. *Tectonics*, *15*(6), 1264–1291. https://doi.org/10.1029/96TC01791

Honegger, K., Dietrich, V., Frank, W., Gansser, A., Thöni, M., & Trommsdorff, V. (1982). Magmatism and metamorphism in the Ladakh Himalayas (the Indus-Tsangpo suture zone). *Earth and Planetary Science Letters*, *60*(2), 253–292. https://doi.org/10.1016/0012-821X(82)90007-3

Hubbard, M., Mukul, M., Gajurel, A. P., Ghosh, A., Srivastava, V., Giri, B., et al. (2021). Orogenic Segmentation and Its Role in Himalayan Mountain Building. *Frontiers in Earth Science*, *9*. Retrieved from https://www.frontiersin.org/articles/10.3389/feart.2021.641666

Jade, S., Shrungeshwara, T. S., Kumar, K., Choudhury, P., Dumka, R. K., & Bhu, H. (2017). India plate angular velocity and contemporary deformation rates from continuous GPS measurements from 1996 to 2015. *Scientific Reports*, *7*(1), 11439. https://doi.org/10.1038/s41598-017-11697-w

Jagoutz, O., Royden, L., Holt, A. F., & Becker, T. W. (2015). Anomalously fast convergence of India and Eurasia caused by double subduction. *Nature Geoscience*, *8*(6), 475–478. https://doi.org/10.1038/ngeo2418

Jain, A. K. (2020). Geological Evolution of the Himalayan Mountains. In N. Gupta & S. K. Tandon (Eds.), *Geodynamics of the Indian Plate: Evolutionary Perspectives* (pp. 363–393). Cham: Springer International Publishing. https://doi.org/10.1007/978-3-030-15989-4_10

Jayangondaperumal, R., Thakur, V. C., Joevivek, V., Rao, P. S., & Gupta, A. K. (2018a). Active Faults of the Kumaun and Garhwal Himalaya. In R. Jayangondaperumal, V. C. Thakur, V. Joevivek, P. S. Rao, & A. K. Gupta (Eds.), *Active Tectonics of Kumaun and Garhwal Himalaya* (pp. 61–141). Singapore: Springer. https://doi.org/10.1007/978-981-10-8243-6_3

Jayangondaperumal, R., Thakur, V. C., Joevivek, V., Rao, P. S., & Gupta, A. K. (2018b). *Active Tectonics of Kumaun and Garhwal Himalaya*. Singapore: Springer. https://doi.org/10.1007/978-981-10-8243-6

Jayangondaperumal, R., Thakur, V. C., Joevivek, V., Rao, P. S., & Gupta, A. K. (2018c). Concluding Comments and Structure of Online Interactive Active Fault Database. In R. Jayangondaperumal, V. C. Thakur, V. Joevivek, P. S. Rao, & A. K. Gupta (Eds.), *Active Tectonics of Kumaun and Garhwal Himalaya* (pp. 143–150). Singapore: Springer. https://doi.org/10.1007/978-981-10-8243-6_4

Johnson, N. M., Stix, J., Tauxe, L., Cerveny, P. F., & Tahirkheli, R. A. K. (1985). Paleomagnetic Chronology, Fluvial Processes, and Tectonic Implications of the Siwalik Deposits near Chinji Village, Pakistan. *The Journal of Geology*, *93*(1), 27–40. Retrieved from https://www.jstor.org/stable/30075201

Jordan, T. A., & Watts, A. B. (2005). Gravity anomalies, flexure and the elastic thickness structure of the India–Eurasia collisional system. *Earth and Planetary Science Letters*, *236*(3), 732–750. https://doi.org/10.1016/j.epsl.2005.05.036

Joshi, L. M., Pant, P. D., Kotlia, B. S., Kothyari, G. C., Luirei, K., & Singh, A. K. (2016). Structural Overview and Morphotectonic Evolution of a Strike-Slip Fault in the Zone of North Almora Thrust, Central Kumaun Himalaya, India. *Journal of Geological Research*, *2016*, e6980943. https://doi.org/10.1155/2016/6980943

Joshi, M., & Tiwari, A. N. (2009). Structural events and metamorphic consequences in Almora Nappe, during Himalayan collision tectonics. *Journal of Asian Earth Sciences*, *34*(3), 326–335. https://doi.org/10.1016/j.jseaes.2008.05.012

Jouanne, F., Mugnier, J. L., Gamond, J. F., Le Fort, P., Pandey, M. R., Bollinger, L., et al. (2004). Current shortening across the Himalayas of Nepal. *Geophysical Journal International*, *157*(1), 1–14. https://doi.org/10.1111/j.1365-246X.2004.02180.x

Kaban, M. K., Tesauro, M., & Cloetingh, S. (2010). An integrated gravity model for Europe's crust and upper mantle. *Earth and Planetary Science Letters*, *296*(3), 195–209. https://doi.org/10.1016/j.epsl.2010.04.041

Karner, G. D., & Watts, A. B. (1983). Gravity anomalies and flexure of the lithosphere at mountain ranges. *Journal of Geophysical Research: Solid Earth*, *88*(B12), 10449–10477. https://doi.org/10.1029/JB088iB12p10449

Kasatkina, E., Koulakov, I., Grapenthin, R., Izbekov, P., Larsen, J. F., Al Arifi, N., & Qaysi, S. I. (2022). Multiple Magma Sources Beneath the Okmok Caldera as Inferred From Local Earthquake Tomography. *Journal of Geophysical Research: Solid Earth*, *127*(10), e2022JB024656. https://doi.org/10.1029/2022JB024656

Kind, R., Yuan, X., Saul, J., Nelson, D., Sobolev, S. V., Mechie, J., et al. (2002). Seismic Images of Crust and Upper Mantle Beneath Tibet: Evidence for Eurasian Plate Subduction. *Science*, *298*(5596), 1219–1221. https://doi.org/10.1126/science.1078115

Klootwijk, C. T., Gee, J. S., Peirce, J. W., & Smith, G. M. (1992). Neogene evolution of the Himalayan-Tibetan region: constraints from ODP site 758, northern ninetyeast ridge; bearing on climatic change. *Palaeogeography, Palaeoclimatology, Palaeoecology*, *95*(1), 95–110. https://doi.org/10.1016/0031-0182(92)90167-4

Kohn, M. J. (2014). Himalayan Metamorphism and Its Tectonic Implications. *Annual Review of Earth and Planetary Sciences*, *42*(1), 381–419. https://doi.org/10.1146/annurev-earth-060313-055005

Kosarev, G., Kind, R., Sobolev, S. V., Yuan, X., Hanka, W., & Oreshin, S. (1999). Seismic Evidence for a Detached Indian Lithospheric Mantle Beneath Tibet. *Science*, *283*(5406), 1306–1309. https://doi.org/10.1126/science.283.5406.1306

Koulakov, I., & Sobolev, S. V. (2006). A tomographic image of Indian lithosphere break-off beneath the Pamir–Hindukush region. *Geophysical Journal International*, *164*(2), 425–440. https://doi.org/10.1111/j.1365-246X.2005.02841.x

Koulakov, I., Maksotova, G., Mukhopadhyay, S., Raoof, J., Kayal, J. R., Jakovlev, A., & Vasilevsky, A. (2015). Variations of the crustal thickness in Nepal Himalayas based on tomographic inversion of regional earthquake data. *Solid Earth*, *6*(1), 207–216. https://doi.org/10.5194/se-6-207-2015

Koulakov, Ivan. (2009a). LOTOS Code for Local Earthquake Tomographic Inversion: Benchmarks for Testing Tomographic Algorithms. *Bulletin of the Seismological Society of America*, *99*(1), 194–214. https://doi.org/10.1785/0120080013

Koulakov, Ivan. (2009b). Out-of-Network Events Can Be of Great Importance for Improving Results of Local Earthquake Tomography. *Bulletin of the Seismological Society of America*, *99*(4), 2556–2563. https://doi.org/10.1785/0120080365

Koulakov, Ivan, Sobolev, S. V., & Asch, G. (2006). P- and S-velocity images of the lithosphere—asthenosphere system in the Central Andes from local-source tomographic inversion. *Geophysical Journal International*, *167*(1), 106–126. https://doi.org/10.1111/j.1365-246X.2006.02949.x

Koulakov, Ivan, Zaharia, B., Enescu, B., Radulian, M., Popa, M., Parolai, S., & Zschau, J. (2010). Delamination or slab detachment beneath Vrancea? New arguments from local earthquake tomography. *Geochemistry, Geophysics, Geosystems*, *11*(3). https://doi.org/10.1029/2009GC002811

Kumar, P., Yuan, X., Kind, R., & Ni, J. (2006). Imaging the colliding Indian and Asian lithospheric plates beneath Tibet. *Journal of Geophysical Research: Solid Earth*, *111*(B6). https://doi.org/10.1029/2005JB003930

Kumar, P., Yuan, X., Kumar, M. R., Kind, R., Li, X., & Chadha, R. K. (2007). The rapid drift of the Indian tectonic plate. *Nature*, *449*(7164), 894–897. https://doi.org/10.1038/nature06214

Kumar, S., Wesnousky, S. G., Rockwell, T. K., Ragona, D., Thakur, V. C., & Seitz, G. G. (2001). Earthquake Recurrence and Rupture Dynamics of Himalayan Frontal Thrust, India. *Science*, *294*(5550), 2328–2331. https://doi.org/10.1126/science.1066195

Kumar, S., Wesnousky, S. G., Rockwell, T. K., Briggs, R. W., Thakur, V. C., & Jayangondaperumal, R. (2006a). Paleoseismic evidence of great surface rupture earthquakes along the Indian Himalaya. *Journal of Geophysical Research: Solid Earth*, *111*(B3). https://doi.org/10.1029/2004JB003309

Kumar, S., Wesnousky, S. G., Rockwell, T. K., Briggs, R. W., Thakur, V. C., & Jayangondaperumal, R. (2006b). Paleoseismic evidence of great surface rupture earthquakes along the Indian Himalaya. *Journal of Geophysical Research: Solid Earth*, *111*(B3). https://doi.org/10.1029/2004JB003309

Kumar, S., Wesnousky, S. G., Jayangondaperumal, R., Nakata, T., Kumahara, Y., & Singh, V. (2010). Paleoseismological evidence of surface faulting along the northeastern Himalayan front, India: Timing, size, and spatial extent of great earthquakes. *Journal of Geophysical Research: Solid Earth*, *115*(B12). https://doi.org/10.1029/2009JB006789

Larson, K. P., Godin, L., & Price, R. A. (2010). Relationships between displacement and distortion in orogens: Linking the Himalayan foreland and hinterland in central Nepal. *GSA Bulletin*, *122*(7–8), 1116–1134. https://doi.org/10.1130/B30073.1

Larson, K. P., Ambrose, T. K., Webb, A. A. G., Cottle, J. M., & Shrestha, S. (2015). Reconciling Himalayan midcrustal discontinuities: The Main Central thrust system. *Earth and Planetary Science Letters*, *429*, 139–146. https://doi.org/10.1016/j.epsl.2015.07.070

Lavé, J., & Avouac, J. P. (2000a). Active folding of fluvial terraces across the Siwaliks Hills, Himalayas of central Nepal. *Journal of Geophysical Research: Solid Earth*, *105*(B3), 5735–5770. https://doi.org/10.1029/1999JB900292

Lavé, J., & Avouac, J. P. (2000b). Active folding of fluvial terraces across the Siwaliks Hills, Himalayas of central Nepal. *Journal of Geophysical Research: Solid Earth*, *105*(B3), 5735–5770. https://doi.org/10.1029/1999JB900292

Lavé, J., & Avouac, J. P. (2001). Fluvial incision and tectonic uplift across the Himalayas of central Nepal. *Journal of Geophysical Research: Solid Earth*, *106*(B11), 26561–26591. https://doi.org/10.1029/2001JB000359

Le Fort, P., Cuney, M., Deniel, C., France-Lanord, C., Sheppard, S. M. F., Upreti, B. N., & Vidal, P. (1987). Crustal generation of the Himalayan leucogranites. *Tectonophysics*, *134*(1), 39–57. https://doi.org/10.1016/0040-1951(87)90248-4

Le Pichon, X., Fournier, M., & Jolivet, L. (1992). Kinematics, topography, shortening, and extrusion in the India-Eurasia collision. *Tectonics*, *11*(6), 1085–1098. https://doi.org/10.1029/92TC01566

Li, J., & Song, X. (2018). Tearing of Indian mantle lithosphere from high-resolution seismic images and its implications for lithosphere coupling in southern Tibet. *Proceedings of the National Academy of Sciences*, *115*(33), 8296–8300. https://doi.org/10.1073/pnas.1717258115

Li, Y., Wang, C., Dai, J., Xu, G., Hou, Y., & Li, X. (2015). Propagation of the deformation and growth of the Tibetan–Himalayan orogen: A review. *Earth-Science Reviews*, *143*, 36–61. https://doi.org/10.1016/j.earscirev.2015.01.001

Liang, X., Zhou, S., Chen, Y. J., Jin, G., Xiao, L., Liu, P., et al. (2008). Earthquake distribution in southern Tibet and its tectonic implications. *Journal of Geophysical Research: Solid Earth*, *113*(B12). https://doi.org/10.1029/2007JB005101

Lin, A. T., & Watts, A. B. (2002). Origin of the West Taiwan basin by orogenic loading and flexure of a rifted continental margin. *Journal of Geophysical Research: Solid Earth*, *107*(B9), ETG 2-1-ETG 2-19. https://doi.org/10.1029/2001JB000669

Malik, J. N., Arora, S., Gadhavi, M. S., Singh, G., Kumar, P., Johnson, F. C., et al. (2023). Geological evidence of paleo-earthquakes on a transverse right-lateral strike-slip fault along the NW Himalayan front: Implications towards fault segmentation and strain partitioning. *Journal of Asian Earth Sciences*, *244*, 105518. https://doi.org/10.1016/j.jseaes.2022.105518

Mandal, P. (2023). The Uttarakhand Himalaya: An image of the main Himalayan thrust, Moho, and lithosphere-asthenosphere boundary. *Journal of Asian Earth Sciences*, *253*, 105724. https://doi.org/10.1016/j.jseaes.2023.105724

Mandal, P., Prathigadapa, R., Srinivas, D., Saha, S., & Saha, G. (2023). Evidence of structural segmentation of the Uttarakhand Himalaya and its implications for earthquake hazard. *Scientific Reports*, *13*(1), 2079. https://doi.org/10.1038/s41598-023-29432-z

Mandal, S., Robinson, D. M., Khanal, S., & Das, O. (2015). Redefining the tectonostratigraphic and structural architecture of the Almora klippe and the Ramgarh–Munsiari thrust sheet in NW India. *Geological Society, London, Special Publications*, *412*(1), 247–269. https://doi.org/10.1144/SP412.6

Martin, A. J. (2017). A review of Himalayan stratigraphy, magmatism, and structure. *Gondwana Research*, *49*, 42–80. https://doi.org/10.1016/j.gr.2017.04.031

Mattauer, M. (1986). Intracontinental subduction, crust-mantle décollement and crustal-stacking wedge in the Himalayas and other collision belts. *Geological Society, London, Special Publications*, *19*(1), 37–50. https://doi.org/10.1144/GSL.SP.1986.019.01.02

Matthews, D., & Hirn, A. (1984). Geophysics: Crustal thickening in Himalayas and Caledonides. *Nature*, *308*(5959), 497–498. https://doi.org/10.1038/308497a0

Medved, I., Koulakov, I., Mukhopadhyay, S., & Jakovlev, A. (2022). Lithosphere structure in the collision zone of the NW Himalayas revealed by alocal earthquake tomography. *Journal of Geodynamics*, *152*, 101922. https://doi.org/10.1016/j.jog.2022.101922

Meigs, A. J., Burbank, D. W., & Beck, R. A. (1995). Middle-late Miocene (>10 Ma) formation of the Main Boundary thrust in the western Himalaya. *Geology*, *23*(5), 423–426. https://doi.org/10.1130/0091-7613(1995)023<0423:MLMMFO>2.3.CO;2

Molnar, P., & Stock, J. M. (2009). Slowing of India's convergence with Eurasia since 20 Ma and its implications for Tibetan mantle dynamics. *Tectonics*, *28*(3). https://doi.org/10.1029/2008TC002271

Molnar, P., & Tapponnier, P. (1975). Cenozoic Tectonics of Asia: Effects of a Continental Collision. *Science*, *189*(4201), 419–426. https://doi.org/10.1126/science.189.4201.419

Molnar, P., & Tapponnier, P. (1977). Relation of the tectonics of eastern China to the India-Eurasia collision: Application of slip-line field theory to large-scale continental tectonics. *Geology*, *5*(4), 212–216. https://doi.org/10.1130/0091-7613(1977)5<212:ROTTOE>2.0.CO;2

Molnar, P., England, P., & Martinod, J. (1993). Mantle dynamics, uplift of the Tibetan Plateau, and the Indian Monsoon. *Reviews of Geophysics*, *31*(4), 357–396. https://doi.org/10.1029/93RG02030

Mugnier, J. L., Leturmy, P., Mascle, G., Huyghe, P., Chalaron, E., Vidal, G., et al. (1999). The Siwaliks of western Nepal: I. Geometry and kinematics. *Journal of Asian Earth Sciences*, *17*(5), 629–642. https://doi.org/10.1016/S1367-9120(99)00038-3

Mugnier, J.-L., Huyghe, P., Chalaron, E., & Mascle, G. (1994). Recent movements along the Main Boundary Thrust of the Himalayas: Normal faulting in an over-critical thrust wedge? *Tectonophysics*, *238*(1), 199–215. https://doi.org/10.1016/0040-1951(94)90056-6

Mukherjee, S., Carosi, R., van der Beek, P., Mukherjee, B. K., & Robinson, D. M. (2015). Tectonics of the Himalaya: an introduction. *Geological Society, London, Special Publications*, *412*(1), 1–3. https://doi.org/10.1144/SP412.14

Mukhopadhyay, B., & Dasgupta, S. (2015). Seismic hazard assessment of Kashmir and Kangra valley region, Western Himalaya, India. *Geomatics, Natural Hazards and Risk*, *6*(2), 149–183. https://doi.org/10.1080/19475705.2013.832405

Mukhopadhyay, S., Koulakov, I., Maksotova, G., Raoof, J., Kayal, J. R., Jakovlev, A., & Vasilevsky, A. (2014). Estimation of Crustal Thickness in Nepal Himalayas Using Local and Regional Earthquake Data, *2014*, S23C-4507. Presented at the AGU Fall Meeting Abstracts. Retrieved from https://ui.adsabs.harvard.edu/abs/2014AGUFM.S23C4507M

Mukhopadhyay, S., Raoof, J., Koulakov, I., & Kayal, J. R. (2016). Seismic Tomography of the Northeast Indian Region: Implications for Underlying Geodynamics, *2016*, T23B-2916. Presented at the AGU Fall Meeting Abstracts. Retrieved from https://ui.adsabs.harvard.edu/abs/2016AGUFM.T23B2916M

Murphy, M. A., Taylor, M. H., Gosse, J., Silver, C. R. P., Whipp, D. M., & Beaumont, C. (2014). Limit of strain partitioning in the Himalaya marked by large earthquakes in western Nepal. *Nature Geoscience*, *7*(1), 38–42. https://doi.org/10.1038/ngeo2017

Murphy, M.A., & Yin, A. (2003). Structural evolution and sequence of thrusting in the Tethyan fold-thrust belt and Indus-Yalu suture zone, southwest Tibet. *GSA Bulletin*, *115*(1), 21–34. https://doi.org/10.1130/0016-7606(2003)115<0021:SEASOT>2.0.CO;2

Murphy, Michael A., & Copeland, P. (2005). Transtensional deformation in the central Himalaya and its role in accommodating growth of the Himalayan orogen. *Tectonics*, *24*(4). https://doi.org/10.1029/2004TC001659

Nábělek, J., Hetényi, G., Vergne, J., Sapkota, S., Kafle, B., Jiang, M., et al. (2009a). Underplating in the Himalaya-Tibet Collision Zone Revealed by the Hi-CLIMB Experiment. *Science*, *325*(5946), 1371–1374. https://doi.org/10.1126/science.1167719

Nábělek, J., Hetényi, G., Vergne, J., Sapkota, S., Kafle, B., Jiang, M., et al. (2009b). Underplating in the Himalaya-Tibet Collision Zone Revealed by the Hi-CLIMB Experiment. *Science*, *325*(5946), 1371–1374. https://doi.org/10.1126/science.1167719

Najman, Yani. (2006). The detrital record of orogenesis: A review of approaches and techniques used in the Himalayan sedimentary basins. *Earth-Science Reviews*, *74*(1), 1–72. https://doi.org/10.1016/j.earscirev.2005.04.004

Najman, Yani, & Garzanti, E. (2000). Reconstructing early Himalayan tectonic evolution and paleogeography from Tertiary foreland basin sedimentary rocks, northern India. *GSA Bulletin*, *112*(3), 435–449. https://doi.org/10.1130/0016-7606(2000)112<435:REHTEA>2.0.CO;2

Najman, Yani, Appel, E., Boudagher-Fadel, M., Bown, P., Carter, A., Garzanti, E., et al. (2010). Timing of India-Asia collision: Geological, biostratigraphic, and palaeomagnetic constraints. *Journal of Geophysical Research: Solid Earth*, *115*(B12). https://doi.org/10.1029/2010JB007673

Najman, Yanina, Clift, P., Johnson, M. R. W., & Robertson, A. H. F. (1993). Early stages of foreland basin evolution in the Lesser Himalaya, N India. *Geological Society, London, Special Publications*, *74*(1), 541–558. https://doi.org/10.1144/GSL.SP.1993.074.01.36

Nakata, T. (1989). Active faults of the Himalaya of India and Nepal. In L. L. Malinconico Jr. & R. J. Lillie (Eds.), *Tectonics of the western Himalayas* (Vol. 232, p. 0). Geological Society of America. https://doi.org/10.1130/SPE232-p243

Nelson, K. D., Zhao, W., Brown, L. D., Kuo, J., Che, J., Liu, X., et al. (1996). Partially Molten Middle Crust Beneath Southern Tibet: Synthesis of Project INDEPTH Results. *Science*, *274*(5293), 1684–1688. https://doi.org/10.1126/science.274.5293.1684

Ni, J., & Barazangi, M. (1984). Seismotectonics of the Himalayan Collision Zone: Geometry of the underthrusting Indian Plate beneath the Himalaya. *Journal of Geophysical Research: Solid Earth*, *89*(B2), 1147–1163. https://doi.org/10.1029/JB089iB02p01147

Nolet, G. (1981). Linearized Inversion of (Teleseismic) Data. In R. Cassinis (Ed.), *The Solution of the Inverse Problem in Geophysical Interpretation* (pp. 9–37). Boston, MA: Springer US. https://doi.org/10.1007/978-1-4684-3962-5_2

Owens, T. J., & Zandt, G. (1997). Implications of crustal property variations for models of Tibetan plateau evolution. *Nature*, *387*(6628), 37–43. https://doi.org/10.1038/387037a0

Paige, C. C., & Saunders, M. A. (1982). LSQR: An Algorithm for Sparse Linear Equations and Sparse Least Squares. *ACM Transactions on Mathematical Software*, *8*(1), 43–71. https://doi.org/10.1145/355984.355989

Pandey, M. R., Tandukar, R. P., Avouac, J. P., Vergne, J., & Héritier, T. (1999). Seismotectonics of the Nepal Himalaya from a local seismic network. *Journal of Asian Earth Sciences*, *17*(5), 703–712. https://doi.org/10.1016/S1367-9120(99)00034-6

Parkash, B., Sharma, R. P., & Roy, A. K. (1980). The Siwalik group (Molasse) — Sediments shed by collision of continental plates. *Sedimentary Geology*, *25*(1), 127–159. https://doi.org/10.1016/0037-0738(80)90058-5

Parrish, R. R., & Hodges, V. (1996a). Isotopic constraints on the age and provenance of the Lesser and Greater Himalayan sequences, Nepalese Himalaya. *GSA Bulletin*, *108*(7), 904–911. https://doi.org/10.1130/0016-7606(1996)108<0904:ICOTAA>2.3.CO;2

Parrish, R. R., & Hodges, V. (1996b). Isotopic constraints on the age and provenance of the Lesser and Greater Himalayan sequences, Nepalese Himalaya. *GSA Bulletin*, *108*(7), 904–911. https://doi.org/10.1130/0016-7606(1996)108<0904:ICOTAA>2.3.CO;2

Patriat, P., & Achache, J. (1984). India–Eurasia collision chronology has implications for crustal shortening and driving mechanism of plates. *Nature*, *311*(5987), 615–621. https://doi.org/10.1038/311615a0

Pearson, O. N., & DeCelles, P. G. (2005). Structural geology and regional tectonic significance of the Ramgarh thrust, Himalayan fold-thrust belt of Nepal. *Tectonics*, *24*(4). https://doi.org/10.1029/2003TC001617

Powers, P. M., Lillie, R. J., & Yeats, R. S. (1998). Structure and shortening of the Kangra and Dehra Dun reentrants, Sub-Himalaya, India. *GSA Bulletin*, *110*(8), 1010–1027. https://doi.org/10.1130/0016-7606(1998)110<1010:SASOTK>2.3.CO;2

Priestley, K., Jackson, J., & McKenzie, D. (2008). Lithospheric structure and deep earthquakes beneath India, the Himalaya and southern Tibet. *Geophysical Journal International*, *172*(1), 345–362. https://doi.org/10.1111/j.1365-246X.2007.03636.x

Pusok, A. E., & Stegman, D. R. (2020). The convergence history of India-Eurasia records multiple subduction dynamics processes. *Science Advances*, *6*(19), eaaz8681. https://doi.org/10.1126/sciadv.aaz8681

Qureshy, M. N. (1998). Major tectonic elements of western Ganga basin. *Current Science*, *74*(10), 820–822. Retrieved from https://www.jstor.org/stable/24101083

Rai, S. S., Priestley, K., Gaur, V. K., Mitra, S., Singh, M. P., & Searle, M. (2006). Configuration of the Indian Moho beneath the NW Himalaya and Ladakh. *Geophysical Research Letters*, *33*(15). https://doi.org/10.1029/2006GL026076

Rajendra Prasad, B., Klemperer, S. L., Vijaya Rao, V., Tewari, H. C., & Khare, P. (2011a). Crustal structure beneath the Sub-Himalayan fold–thrust belt, Kangra recess, northwest India, from seismic reflection profiling: Implications for Late Paleoproterozoic orogenesis and modern earthquake hazard. *Earth and Planetary Science Letters*, *308*(1), 218–228. https://doi.org/10.1016/j.epsl.2011.05.052

Rajendra Prasad, B., Klemperer, S. L., Vijaya Rao, V., Tewari, H. C., & Khare, P. (2011b). Crustal structure beneath the Sub-Himalayan fold–thrust belt, Kangra recess, northwest India, from seismic reflection profiling: Implications for Late Paleoproterozoic orogenesis and modern earthquake hazard. *Earth and Planetary Science Letters*, *308*(1), 218–228. https://doi.org/10.1016/j.epsl.2011.05.052

Raoof, J., Mukhopadhyay, S., Koulakov, I., & Kayal, J. R. (2017). 3-D seismic tomography of the lithosphere and its geodynamic implications beneath the northeast India region. *Tectonics*, *36*(5), 962–980. https://doi.org/10.1002/2016TC004375

Raoof, J., Mukhopadhyay, S., & Malik, J. N. (2018). 3-D Seismic Tomography of the Indo-Asian Collision Zone from Pamir-Hindu Kush in the West to Indo-Burma Ranges in the East: Geodynamic Implications, *2018*, T23B-0366. Presented at the AGU Fall Meeting Abstracts. Retrieved from https://ui.adsabs.harvard.edu/abs/2018AGUFM.T23B0366R

Raoof, Javed, Malik, J. N., & Mukhopadhyay, S. (2019). Seismic Tomography of the Lithosphere beneath the Nepal Himalayas and Geodynamic Implications for 2015 Gorkha Earthquake, 602. Presented at the EGU General Assembly Conference Abstracts. Retrieved from https://ui.adsabs.harvard.edu/abs/2019EGUGA..21..602R

Ratschbacher, L., Frisch, W., Liu, G., & Chen, C. (1994). Distributed deformation in southern and western Tibet during and after the India-Asia collision. *Journal of Geophysical Research: Solid Earth*, *99*(B10), 19917–19945. https://doi.org/10.1029/94JB00932

Relation of gravity to elevation and rejuvenation of blocks in India. (1971). *Journal of Geophysical Research (1896-1977)*, *76*(2), 545–557. https://doi.org/10.1029/JB076i002p00545

Replumaz, A., Kárason, H., van der Hilst, R. D., Besse, J., & Tapponnier, P. (2004). 4-D evolution of SE Asia's mantle from geological reconstructions and seismic tomography. *Earth and Planetary Science Letters*, *221*(1), 103–115. https://doi.org/10.1016/S0012-821X(04)00070-6

Replumaz, A., Negredo, A. M., Guillot, S., der Beek, P. van, & Villaseñor, A. (2010). Crustal mass budget and recycling during the India/Asia collision. *Tectonophysics*, *492*(1), 99–107. https://doi.org/10.1016/j.tecto.2010.05.023

Replumaz, A., Negredo, A. M., Villaseñor, A., & Guillot, S. (2010). Indian continental subduction and slab break-off during Tertiary collision. *Terra Nova*, *22*(4), 290–296. https://doi.org/10.1111/j.1365-3121.2010.00945.x

Replumaz, A., Negredo, A. M., Guillot, S., & Villaseñor, A. (2010). Multiple episodes of continental subduction during India/Asia convergence: Insight from seismic tomography and tectonic reconstruction. *Tectonophysics*, *483*(1), 125–134. https://doi.org/10.1016/j.tecto.2009.10.007

Replumaz, A., Guillot, S., Villaseñor, A., & Negredo, A. M. (2013). Amount of Asian lithospheric mantle subducted during the India/Asia collision. *Gondwana Research*, *24*(3), 936–945. https://doi.org/10.1016/j.gr.2012.07.019

Replumaz, A., Capitanio, F. A., Guillot, S., Negredo, A. M., & Villaseñor, A. (2014). The coupling of Indian subduction and Asian continental tectonics. *Gondwana Research*, *26*(2), 608–626. https://doi.org/10.1016/j.gr.2014.04.003

Reuber, I. (1986). Geometry of accretion and oceanic thrusting of the Spongtang Ophiolite, Ladakh-Himalaya. *Nature*, *321*(6070), 592–596. https://doi.org/10.1038/321592a0

Reuber, I. (1989). The Dras arc: two successive volcanic events on eroded oceanic crust. *Tectonophysics*, *161*(1), 93–106. https://doi.org/10.1016/0040-1951(89)90305-3

Reuber, I., Colchen, M., & Mevel, C. (1987). The geodynamic evolution of the South-Tethyan, margin in Zanskar, NW-Himalaya, as revealed by the Spongtang ophiolitic melanges. *Geodinamica Acta*, *1*(4–5), 283–296. https://doi.org/10.1080/09853111.1987.11105146

Robert, X., van der Beek, P., Braun, J., Perry, C., & Mugnier, J.-L. (2011). Control of detachment geometry on lateral variations in exhumation rates in the Himalaya: Insights from low-temperature thermochronology and numerical modeling. *Journal of Geophysical Research: Solid Earth*, *116*(B5). https://doi.org/10.1029/2010JB007893

Robertson, A., & Degnan, P. (1994). The Dras arc Complex: lithofacies and reconstruction of a Late Cretaceous oceanic volcanic arc in the Indus Suture Zone, Ladakh Himalaya. *Sedimentary Geology*, *92*(1), 117–145. https://doi.org/10.1016/0037-0738(94)90057-4

Robertson, A. H. F., & Degnan, P. J. (1993). Sedimentology and tectonic implications of the Lamayuru Complex: deep-water facies of the Indian passive margin, Indus Suture Zone, Ladakh Himalaya. *Geological Society, London, Special Publications*, *74*(1), 299–321. https://doi.org/10.1144/GSL.SP.1993.074.01.21

Robinson, D. M., DeCelles, P. G., & Copeland, P. (2006a). Tectonic evolution of the Himalayan thrust belt in western Nepal: Implications for channel flow models. *GSA Bulletin*, *118*(7–8), 865–885. https://doi.org/10.1130/B25911.1

Robinson, D. M., DeCelles, P. G., & Copeland, P. (2006b). Tectonic evolution of the Himalayan thrust belt in western Nepal: Implications for channel flow models. *GSA Bulletin*, *118*(7–8), 865–885. https://doi.org/10.1130/B25911.1

Royden, L. H., Burchfiel, B. C., & van der Hilst, R. D. (2008). The Geological Evolution of the Tibetan Plateau. *Science*, *321*(5892), 1054–1058. https://doi.org/10.1126/science.1155371

SCAILLET, B., PICHAVANT, M., & ROUX, J. (1995). Experimental Crystallization of Leucogranite Magmas. *Journal of Petrology*, *36*(3), 663–705. https://doi.org/10.1093/petrology/36.3.663

Schelling, D., & Arita, K. (1991). Thrust tectonics, crustal shortening, and the structure of the far-eastern Nepal Himalaya. *Tectonics*, *10*(5), 851–862. https://doi.org/10.1029/91TC01011

Searle, M., Corfield, R. I., Stephenson, B., & Mccarron, J. (1997). Structure of the North Indian continental margin in the Ladakh–Zanskar Himalayas: implications for the timing of obduction of the Spontang ophiolite, India–Asia collision and deformation events in the Himalaya. *Geological Magazine*, *134*(3), 297–316. https://doi.org/10.1017/S0016756897006857

Searle, M. P. (1986). Structural evolution and sequence of thrusting in the High Himalayan, Tibetan—Tethys and Indus suture zones of Zanskar and Ladakh, Western Himalaya. *Journal of Structural Geology*, *8*(8), 923–936. https://doi.org/10.1016/0191-8141(86)90037-4

Searle, M. P. (1999). Emplacement of Himalayan leucogranites by magma injection along giant sill complexes: examples from the Cho Oyu, Gyachung Kang and Everest leucogranites (Nepal Himalaya). *Journal of Asian Earth Sciences*, *17*(5), 773–783. https://doi.org/10.1016/S1367-9120(99)00020-6

Searle, M. P., & Treloar, P. J. (1993). Himalayan Tectonics — an introduction. *Geological Society, London, Special Publications*, *74*(1), 1–7. https://doi.org/10.1144/GSL.SP.1993.074.01.01

Searle, Michael P., & Treloar, P. J. (2019). Introduction to Himalayan tectonics: a modern synthesis. *Geological Society, London, Special Publications*, *483*(1), 1–17. https://doi.org/10.1144/SP483-2019-20

Seeber, L., & Armbruster, J. G. (1981). Great Detachment Earthquakes Along the Himalayan Arc and Long-Term Forecasting. In *Earthquake Prediction* (pp. 259–277). American Geophysical Union (AGU). https://doi.org/10.1029/ME004p0259

Sella, G. F., Dixon, T. H., & Mao, A. (2002). REVEL: A model for Recent plate velocities from space geodesy. *Journal of Geophysical Research: Solid Earth*, *107*(B4), ETG 11-1-ETG 11-30. https://doi.org/10.1029/2000JB000033

Sharma, K. K. (1998). Geologic and tectonic evolution of the Himalaya before and after the India-Asia collision. *Proceedings of the Indian Academy of Sciences - Earth and Planetary Sciences*, *107*(4), 265–282. https://doi.org/10.1007/BF02841594

de Sigoyer, J., Chavagnac, V., Blichert-Toft, J., Villa, I. M., Luais, B., Guillot, S., et al. (2000). Dating the Indian continental subduction and collisional thickening in the northwest Himalaya: Multichronology of the Tso Morari eclogites. *Geology*, *28*(6), 487–490. https://doi.org/10.1130/0091-7613(2000)28<487:DTICSA>2.0.CO;2

Singh, A. P., Koulakov, I., Kumar, M. R., Kumar, S., & Kayal, J. R. (2019). Seismic velocity structure and intraplate seismicity beneath the Deccan Volcanic Province of western India. *Physics of the Earth and Planetary Interiors*, *287*, 21–36. https://doi.org/10.1016/j.pepi.2018.12.007

Sinha, A. K. (1987). Tectonic zonation of the Central Himalaya and the crustal evolution of collision and compressional belts. *Tectonophysics*, *134*(1), 59–74. https://doi.org/10.1016/0040-1951(87)90249-6

van der Sluis, A., & van der Vorst, H. A. (1987). Numerical solution of large, sparse linear algebraic systems arising from tomographic problems. In G. Nolet (Ed.), *Seismic Tomography: With Applications in Global Seismology and Exploration Geophysics* (pp. 49–83). Dordrecht: Springer Netherlands. https://doi.org/10.1007/978-94-009-3899-1_3

Srivastava, P., & Mitra, G. (1994a). Thrust geometries and deep structure of the outer and lesser Himalaya, Kumaon and Garhwal (India): Implications for evolution of the Himalayan fold-and-thrust belt. *Tectonics*, *13*(1), 89–109. https://doi.org/10.1029/93TC01130

Srivastava, P., & Mitra, G. (1994b). Thrust geometries and deep structure of the outer and lesser Himalaya, Kumaon and Garhwal (India): Implications for evolution of the Himalayan fold-and-thrust belt. *Tectonics*, *13*(1), 89–109. https://doi.org/10.1029/93TC01130

Stevens, V. L., & Avouac, J. P. (2015a). Interseismic coupling on the main Himalayan thrust. *Geophysical Research Letters*, *42*(14), 5828–5837. https://doi.org/10.1002/2015GL064845

Stevens, V. L., & Avouac, J. P. (2015b). Interseismic coupling on the main Himalayan thrust. *Geophysical Research Letters*, *42*(14), 5828–5837. https://doi.org/10.1002/2015GL064845

Streule, M. J., Searle, M. P., Waters, D. J., & Horstwood, M. S. A. (2010). Metamorphism, melting, and channel flow in the Greater Himalayan Sequence and Makalu leucogranite: Constraints from thermobarometry, metamorphic modeling, and U-Pb geochronology. *Tectonics*, *29*(5). https://doi.org/10.1029/2009TC002533

Sychev, I. V., Koulakov, I., Sycheva, N. A., Koptev, A., Medved, I., El Khrepy, S., & Al-Arifi, N. (2018). Collisional Processes in the Crust of the Northern Tien Shan Inferred From Velocity and Attenuation Tomography Studies. *Journal of Geophysical Research: Solid Earth*, *123*(2), 1752–1769. https://doi.org/10.1002/2017JB014826

Szeliga, W., Hough, S., Martin, S., & Bilham, R. (2010). Intensity, Magnitude, Location, and Attenuation in India for Felt Earthquakes since 1762. *Bulletin of the Seismological Society of America*, *100*(2), 570–584. https://doi.org/10.1785/0120080329

Talebi, A., Koulakov, I., Moradi, A., Rahimi, H., & Gerya, T. (2020). Ongoing formation of felsic lower crustal channel by relamination in Zagros collision zone revealed from regional tomography. *Scientific Reports*, *10*(1), 8224. https://doi.org/10.1038/s41598-020-64946-w

Tan, P., Liang, X., Li, W., & Wu, C. (2023). Crustal structure of the Tibetan Plateau and adjacent areas revealed from ambient noise tomography. *Gondwana Research*, *121*, 1–15. https://doi.org/10.1016/j.gr.2023.03.029

Tapponnier, P., Peltzer, G., & Armijo, R. (1986). On the mechanics of the collision between India and Asia. *Geological Society, London, Special Publications*, *19*(1), 113–157. https://doi.org/10.1144/GSL.SP.1986.019.01.07

Tapponnier, Paul, Zhiqin, X., Roger, F., Meyer, B., Arnaud, N., Wittlinger, G., & Jingsui, Y. (2001). Oblique Stepwise Rise and Growth of the Tibet Plateau. *Science*, *294*(5547), 1671–1677. https://doi.org/10.1126/science.105978

Thakur, V. C., Jayangondaperumal, R., & Joevivek, V. (2019). Seismotectonics of central and NW Himalaya: plate boundary–wedge thrust earthquakes in thin- and thick-skinned tectonic framework. *Geological Society, London, Special Publications*, *481*(1), 41–63. https://doi.org/10.1144/SP481.8

Thakur, Vikram C. (1987). Development of major structures across the northwestern Himalaya, India. *Tectonophysics*, *135*(1), 1–13. https://doi.org/10.1016/0040-1951(87)90147-8

Treloar, P. J., & Coward, M. P. (1991). Indian Plate motion and shape: constraints on the geometry of the Himalayan orogen. *Tectonophysics*, *191*(3), 189–198. https://doi.org/10.1016/0040-1951(91)90055-W

Um, J., & Thurber, C. (1987). A fast algorithm for two-point seismic ray tracing. *Bulletin of the Seismological Society of America*, *77*(3), 972–986. https://doi.org/10.1785/BSSA0770030972

Upreti, B. N. (1999). An overview of the stratigraphy and tectonics of the Nepal Himalaya. *Journal of Asian Earth Sciences*, *17*(5), 577–606. https://doi.org/10.1016/S1367-9120(99)00047-4

Valdiya, K. S. (1976). Himalayan transverse faults and folds and their parallelism with subsurface structures of North Indian plains. *Tectonophysics*, *32*(3), 353–386. https://doi.org/10.1016/0040-1951(76)90069-X

Valdiya, K. S., & Kotlia, B. S. (2001). Fluvial Geomorphic Evidence for Late Quaternary Reactivation of a Synclinally Folded Nappe in Kumaun Lesser Himalaya. *Geological Society of India*, *58*(4), 303–317. Retrieved from https://www.samvad.sibmpune.edu.in/index.php/jgsi/article/view/83798

Valdiya, K. S., Cronin, V. S., Shackleton, R. M., Dewey, J. F., & Windley, B. F. (1997). Tectonics and evolution of the central sector of the Himalaya. *Philosophical Transactions of the Royal Society of London. Series A, Mathematical and Physical Sciences*, *326*(1589), 151–175. https://doi.org/10.1098/rsta.1988.0083

Van der Voo, R., Spakman, W., & Bijwaard, H. (1999). Mesozoic subducted slabs under Siberia. *Nature*, *397*(6716), 246–249. https://doi.org/10.1038/16686

Vance, D., Bickle, M., Ivy-Ochs, S., & Kubik, P. W. (2003). Erosion and exhumation in the Himalaya from cosmogenic isotope inventories of river sediments. *Earth and Planetary Science Letters*, *206*(3), 273–288. https://doi.org/10.1016/S0012-821X(02)01102-0

Verma, R. K., & Mukhopadhyay, M. (1977). An analysis of the gravity field in Northeastern India. *Tectonophysics*, *42*(2), 283–317. https://doi.org/10.1016/0040-1951(77)90171-8

Verma, R. K., Mukhopadhyay, M., & Ahluwalia, M. S. (1976). Seismicity, gravity, and tectonics of northeast India and northern Burma. *Bulletin of the Seismological Society of America*, *66*(5), 1683–1694. https://doi.org/10.1785/BSSA0660051683

Vijaya Rao, V., Rajendra Prasad, B., Reddy, P. R., & Tewari, H. C. (2000). Evolution of Proterozoic Aravalli Delhi Fold Belt in the northwestern Indian Shield from seismic studies. *Tectonophysics*, *327*(1), 109–130. https://doi.org/10.1016/S0040-1951(00)00156-6

Watts, A. B., & Daly, S. F. (1981). Long Wavelength Gravity and Topography Anomalies. *Annual Review of Earth and Planetary Sciences*, *9*(1), 415–448. https://doi.org/10.1146/annurev.ea.09.050181.002215

Webb, A. A. G., Yin, A., Harrison, T. M., Célérier, J., & Burgess, W. P. (2007). The leading edge of the Greater Himalayan Crystalline complex revealed in the NW Indian Himalaya: Implications for the evolution of the Himalayan orogen. *Geology*, *35*(10), 955–958. https://doi.org/10.1130/G23931A.1

Webb, A. A. G., Schmitt, A. K., He, D., & Weigand, E. L. (2011). Structural and geochronological evidence for the leading edge of the Greater Himalayan Crystalline complex in the central Nepal Himalaya. *Earth and Planetary Science Letters*, *304*(3), 483–495. https://doi.org/10.1016/j.epsl.2011.02.024

Wesnousky, S. G., Kumar, S., Mohindra, R., & Thakur, V. C. (1999). Uplift and convergence along the Himalayan Frontal Thrust of India. *Tectonics*, *18*(6), 967–976. https://doi.org/10.1029/1999TC900026

Whipp Jr., D. M., Ehlers, T. A., Blythe, A. E., Huntington, K. W., Hodges, K. V., & Burbank, D. W. (2007). Plio-Quaternary exhumation history of the central Nepalese Himalaya: 2. Thermokinematic and thermochronometer age prediction model. *Tectonics*, *26*(3). https://doi.org/10.1029/2006TC001991

White, L. T., & Lister, G. S. (2012). The collision of India with Asia. *Journal of Geodynamics*, *56–57*, 7–17. https://doi.org/10.1016/j.jog.2011.06.006

Wittlinger, G., Vergne, J., Tapponnier, P., Farra, V., Poupinet, G., Jiang, M., et al. (2004). Teleseismic imaging of subducting lithosphere and Moho offsets beneath western Tibet. *Earth and Planetary Science Letters*, *221*(1), 117–130. https://doi.org/10.1016/S0012-821X(03)00723-4

Wu, C., Nelson, K. D., Wortman, G., Samson, S. D., Yue, Y., Li, J., et al. (1998). Yadong cross structure and South Tibetan Detachment in the east central Himalaya (89°–90°E). *Tectonics*, *17*(1), 28–45. https://doi.org/10.1029/97TC03386

Wu, Y., Bao, X., Zhang, B., Xu, Y., & Yang, W. (2022). Seismic Evidence for Stepwise Lithospheric Delamination Beneath the Tibetan Plateau. *Geophysical Research Letters*, *49*(10), e2022GL098528. https://doi.org/10.1029/2022GL098528

Xu, Q., Zhao, J., Yuan, X., Liu, H., & Pei, S. (2017). Detailed Configuration of the Underthrusting Indian Lithosphere Beneath Western Tibet Revealed by Receiver Function Images. *Journal of Geophysical Research: Solid Earth*, *122*(10), 8257–8269. https://doi.org/10.1002/2017JB014490

Yadav, R. K., Gahalaut, V. K., Bansal, A. K., Sati, S. P., Catherine, J., Gautam, P., et al. (2019). Strong seismic coupling underneath Garhwal–Kumaun region, NW Himalaya, India. *Earth and Planetary Science Letters*, *506*, 8–14. https://doi.org/10.1016/j.epsl.2018.10.023

Yadav, R. K., Gahalaut, V. K., & Bansal, A. K. (2021). Tectonic and non-tectonic crustal deformation in Kumaun Garhwal Himalaya. *Quaternary International*, *585*, 171–182. https://doi.org/10.1016/j.quaint.2020.10.011

Yang, T., Jin, J., Bian, W., Ma, Y., Gao, F., Peng, W., et al. (2019). Precollisional Latitude of the Northern Tethyan Himalaya From the Paleocene Redbeds and Its Implication for Greater India and the India-Asia collision. *Journal of Geophysical Research: Solid Earth*, *124*(11), 10777–10798. https://doi.org/10.1029/2019JB017927

Yin, A. (2006). Cenozoic tectonic evolution of the Himalayan orogen as constrained by along-strike variation of structural geometry, exhumation history, and foreland sedimentation. *Earth-Science Reviews*, *76*(1), 1–131. https://doi.org/10.1016/j.earscirev.2005.05.004

Yin, A., & Harrison, T. M. (2000). Geologic Evolution of the Himalayan-Tibetan Orogen. *Annual Review of Earth and Planetary Sciences*, *28*(1), 211–280. https://doi.org/10.1146/annurev.earth.28.1.211

Yin, A., Dubey, C. S., Kelty, T. K., Webb, A. A. G., Harrison, T. M., Chou, C. Y., & Célérier, J. (2010). Geologic correlation of the Himalayan orogen and Indian craton: Part 2. Structural geology, geochronology, and tectonic evolution of the Eastern Himalaya. *GSA Bulletin*, *122*(3–4), 360–395. https://doi.org/10.1130/B26461.1

Zhang, J., Santosh, M., Wang, X., Guo, L., Yang, X., & Zhang, B. (2012). Tectonics of the northern Himalaya since the India–Asia collision. *Gondwana Research*, *21*(4), 939–960. https://doi.org/10.1016/j.gr.2011.11.004

Zhang, Z., Wang, Y., Houseman, G. A., Xu, T., Wu, Z., Yuan, X., et al. (2014). The Moho beneath western Tibet: Shear zones and eclogitization in the lower crust. *Earth and Planetary Science Letters*, *408*, 370–377. https://doi.org/10.1016/j.epsl.2014.10.022

Zhao, D., Wang, Z., Umino, N., & Hasegawa, A. (2007). Tomographic Imaging outside a Seismic Network: Application to the Northeast Japan Arc. *Bulletin of the Seismological Society of America*, *97*(4), 1121–1132. https://doi.org/10.1785/0120050256

Zhao, W., Nelson, K. D., Che, J., Quo, J., Lu, D., Wu, C., & Liu, X. (1993a). Deep seismic reflection evidence for continental underthrusting beneath southern Tibet. *Nature*, *366*(6455), 557–559. https://doi.org/10.1038/366557a0

Zhao, W., Nelson, K. D., Che, J., Quo, J., Lu, D., Wu, C., & Liu, X. (1993b). Deep seismic reflection evidence for continental underthrusting beneath southern Tibet. *Nature*, *366*(6455), 557–559. https://doi.org/10.1038/366557a0

Zhou, H., & Murphy, M. A. (2005). Tomographic evidence for wholesale underthrusting of India beneath the entire Tibetan plateau. *Journal of Asian Earth Sciences*, *25*(3), 445–457. https://doi.org/10.1016/j.jseaes.2004.04.007

Figure 1: Tectonic Map of the study region.

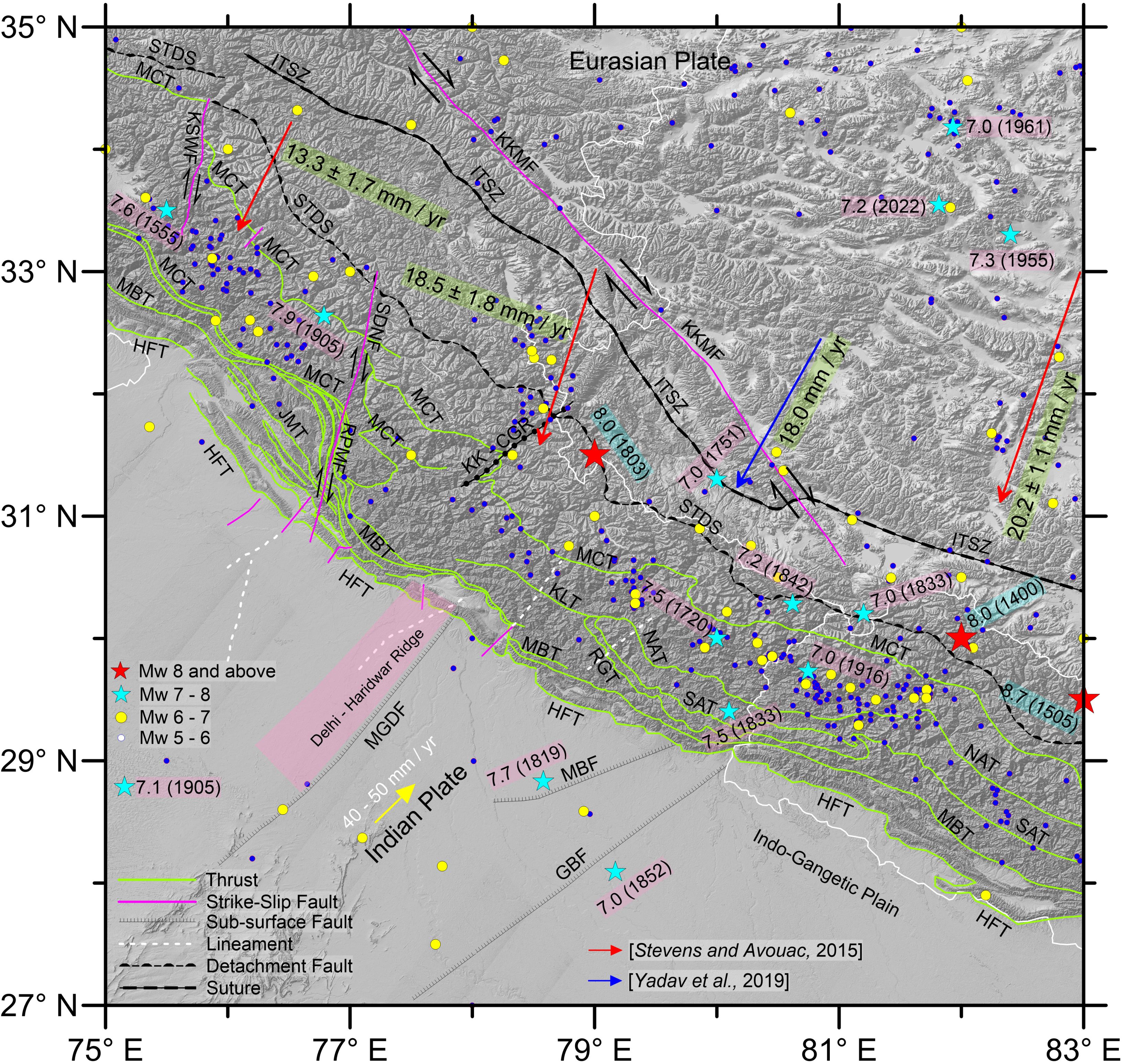

35° N
33° N
31° N
29° N
27° N
75° E
77° E
79° E
81° E
83° E
Eurasian Plate
Indian Plate
Indo-Gangetic Plain
Delhi - Haridwar Ridge
13.3 ± 1.7 mm / yr
18.5 ± 1.8 mm / yr
18.0 mm / yr
20.2 ± 1.1 mm / yr
40 - 50 mm / yr
STDS
ITSZ
MCT
KSWF
KKMF
SDNF
RPMF
JMT
MBT
HFT
KK - CGR
KLT
NAT
RGT
SAT
MGDF
MBF
GBF
7.6 (1555)
7.9 (1905)
8.0 (1803)
7.0 (1751)
7.2 (1842)
7.5 (1720)
7.0 (1833)
8.0 (1400)
7.0 (1916)
8.7 (1505)
7.5 (1833)
7.7 (1819)
7.0 (1852)
7.1 (1905)
7.0 (1961)
7.2 (2022)
7.3 (1955)
Mw 8 and above
Mw 7 - 8
Mw 6 - 7
Mw 5 - 6
Thrust
Strike-Slip Fault
Sub-surface Fault
Lineament
Detachment Fault
Suture
[Stevens and Avouac, 2015]
[Yadav et al., 2019]

Figure 2: Data distribution.

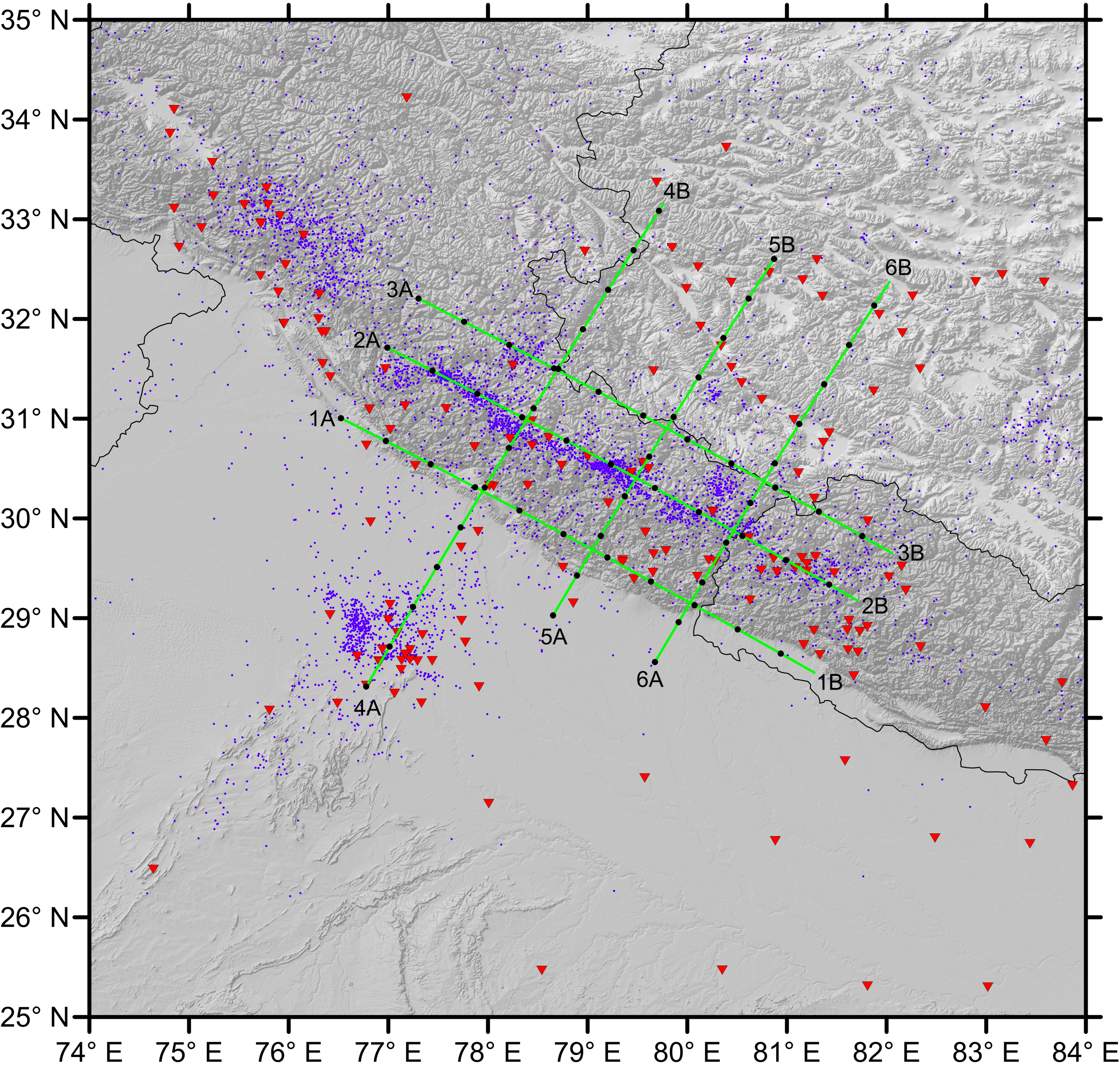

35° N
34° N
33° N
32° N
31° N
30° N
29° N
28° N
27° N
26° N
25° N
74° E
75° E
76° E
77° E
78° E
79° E
80° E
81° E
82° E
83° E
84° E
1A
1B
2A
2B
3A
3B
4A
4B
5A
5B
6A
6B

Figure 3: Preliminary 1-D Reference Velocity Models.

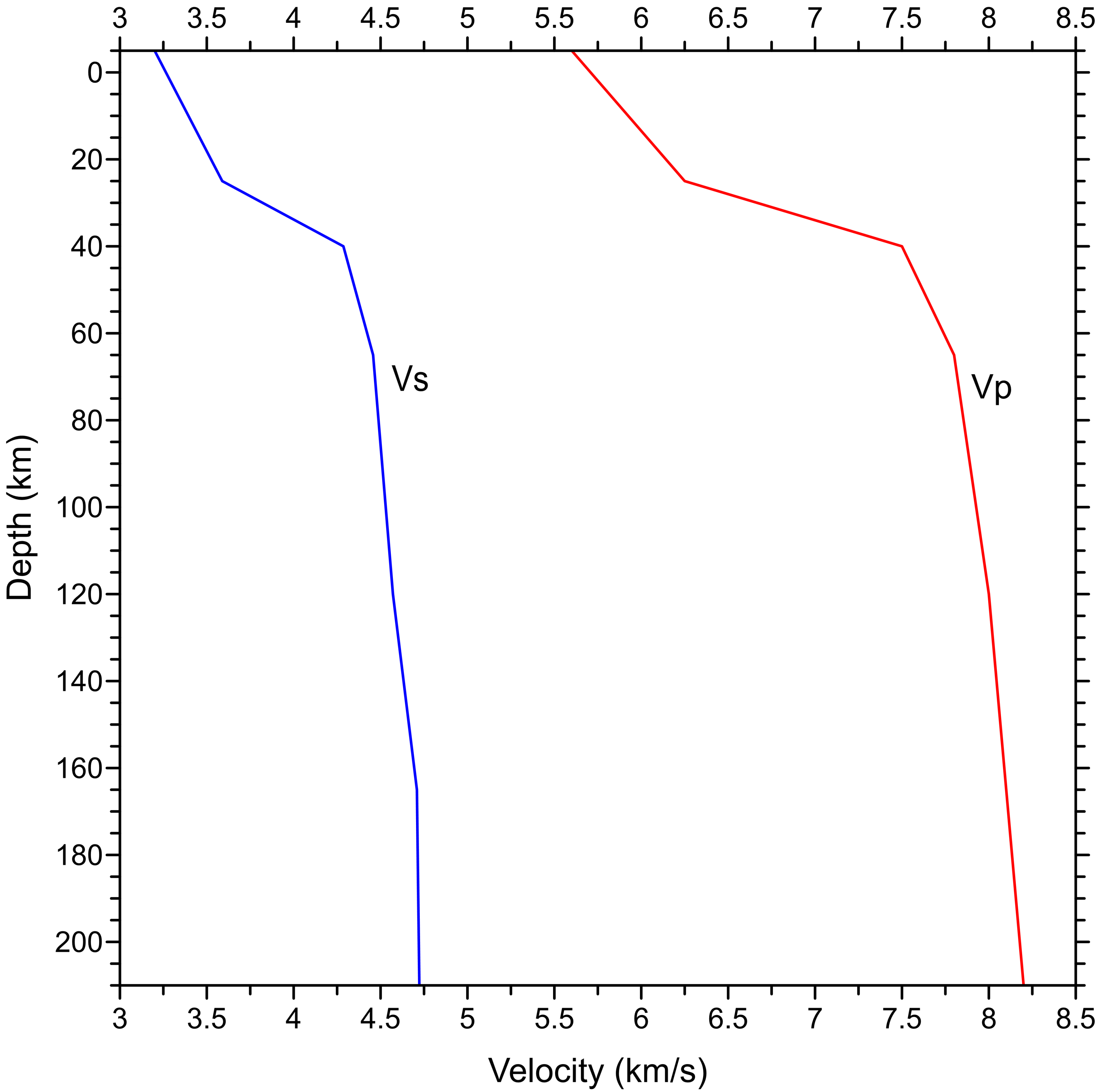

3
3.5
4
4.5
5
5.5
6
6.5
7
7.5
8
8.5
0
20
40
60
80
100
120
140
160
180
200
Depth (km)
Vs
Vp
Velocity (km/s)

Figure 4: Synthetic test through free shape anomalies.

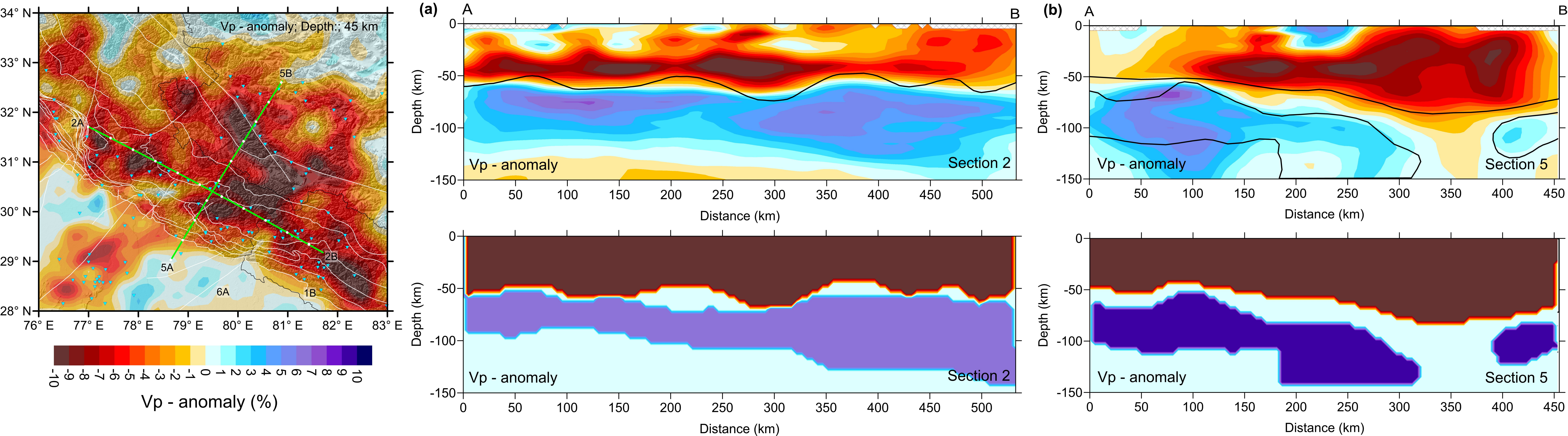

Vp - anomaly; Depth:; 45 km
34° N
33° N
32° N
31° N
30° N
29° N
28° N
76° E
77° E
78° E
79° E
80° E
81° E
82° E
83° E
2A
2B
5A
5B
6A
1B
-10 -9 -8 -7 -6 -5 -4 -3 -2 -1 0 1 2 3 4 5 6 7 8 9 10
Vp - anomaly (%)
(a)
A
B
Depth (km)
Distance (km)
Vp - anomaly
Section 2
(b)
Section 5

Figure 5: Vertical Checkerboard test.

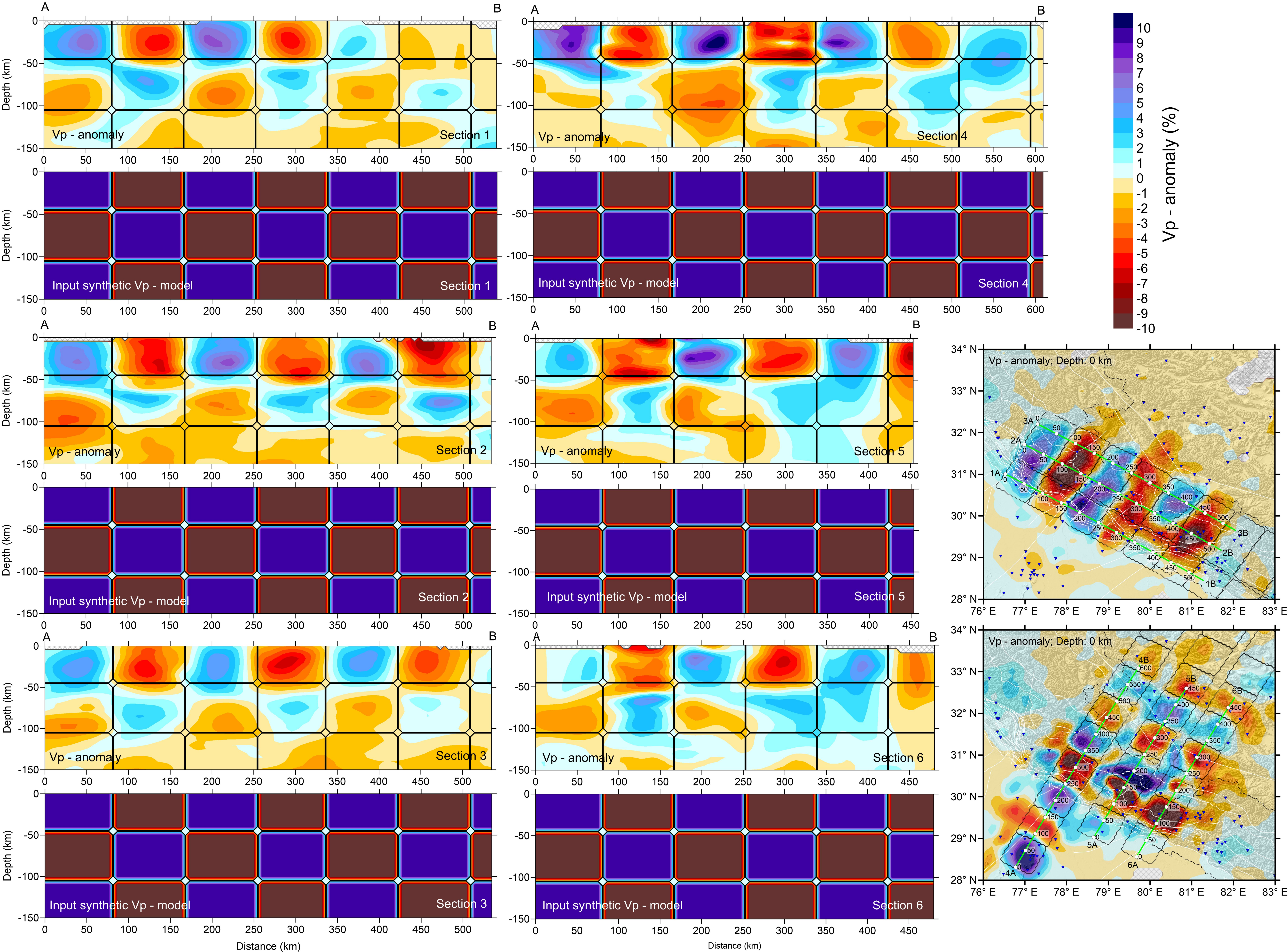

Vp - anomaly
Input synthetic Vp - model
Section 1
Section 2
Section 3
Section 4
Section 5
Section 6
Depth (km)
Distance (km)
Vp - anomaly (%)
Vp - anomaly; Depth: 0 km

Figure 6: Horizontal Slices of Vp - anomalies.

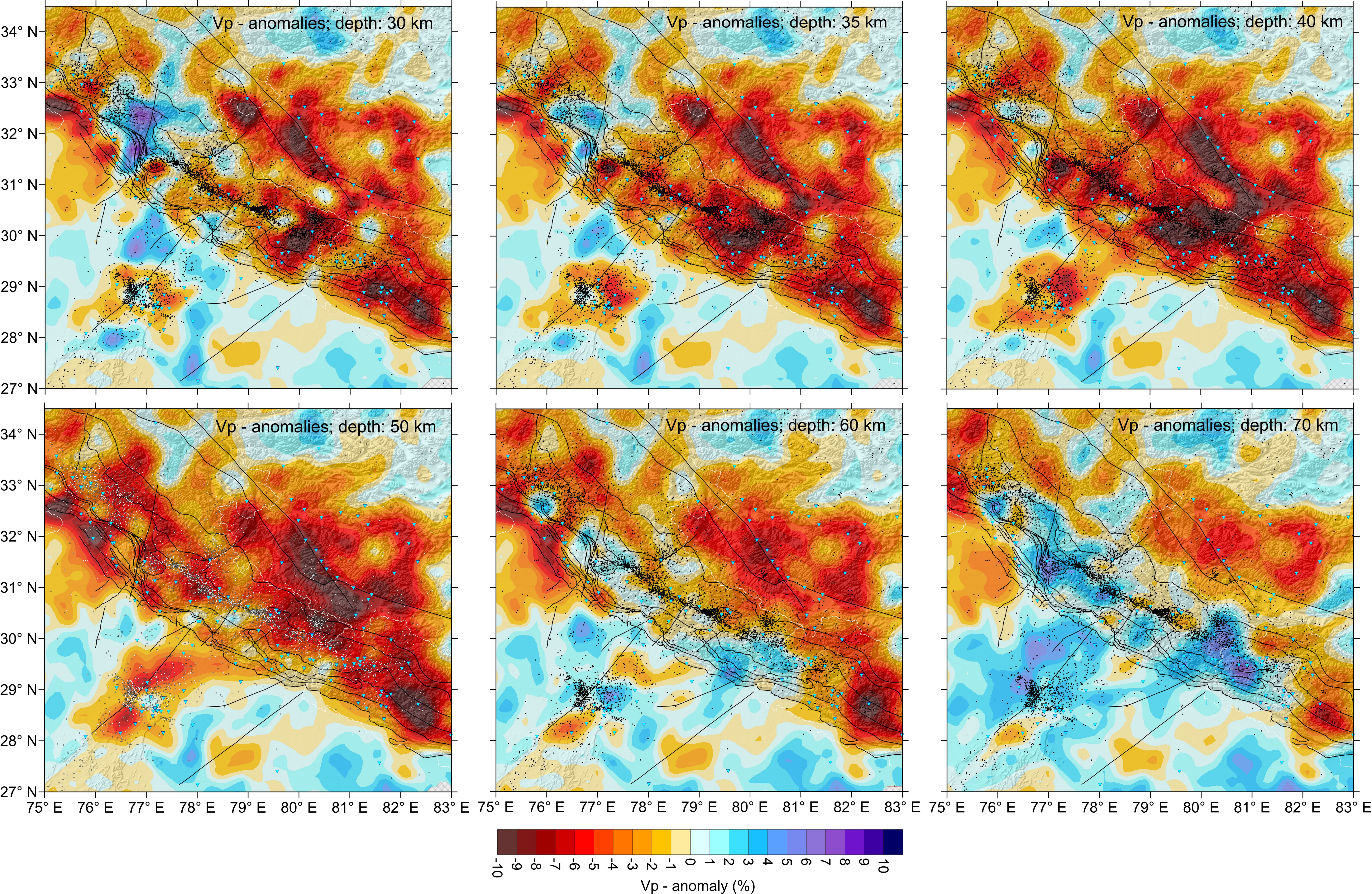
Vp - anomalies; depth: 30 km
Vp - anomalies; depth: 35 km
Vp - anomalies; depth: 40 km
Vp - anomalies; depth: 50 km
Vp - anomalies; depth: 60 km
Vp - anomalies; depth: 70 km
34° N
33° N
32° N
31° N
30° N
29° N
28° N
27° N
75° E
76° E
77° E
78° E
79° E
80° E
81° E
82° E
83° E
-10 -9 -8 -7 -6 -5 -4 -3 -2 -1 0 1 2 3 4 5 6 7 8 9 10
Vp - anomaly (%)

Figure 7: Cross-sections of Vp - anomalies.

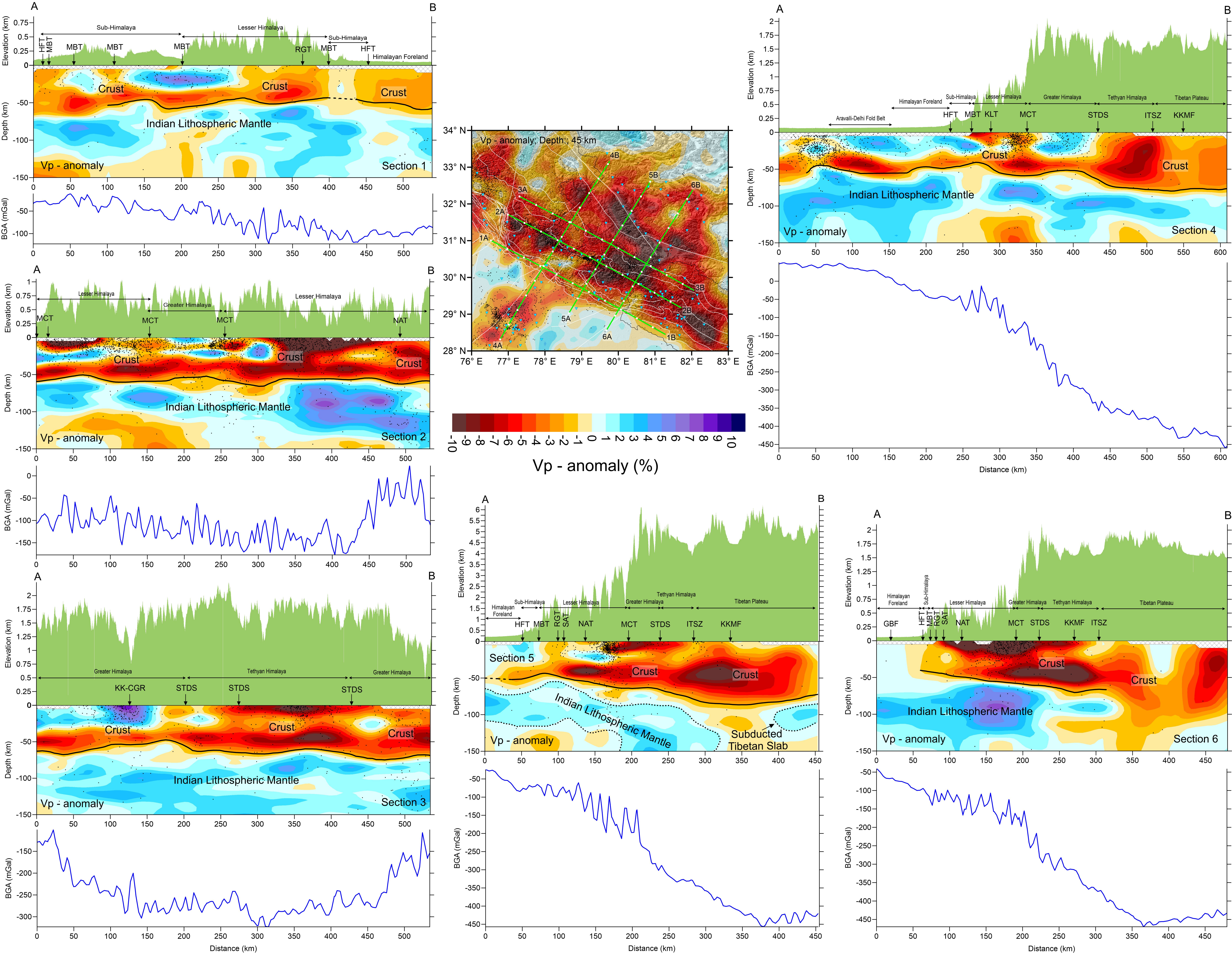

Section 1
Section 2
Section 3
Section 4
Section 5
Section 6
Vp - anomaly
Crust
Indian Lithospheric Mantle
Subducted Tibetan Slab
Vp - anomaly; Depth: 45 km
Vp - anomaly (%)
Elevation (km)
Depth (km)
BGA (mGal)
Distance (km)
Sub-Himalaya
Lesser Himalaya
Greater Himalaya
Tethyan Himalaya
Tibetan Plateau
Himalayan Foreland
Aravalli-Delhi Fold Belt
HFT
MBT
MCT
RGT
SAT
NAT
KLT
STDS
ITSZ
KKMF
KK-CGR
GBF

Figure 8: Cross-sections of Vp - anomalies along profiles selected from literature.

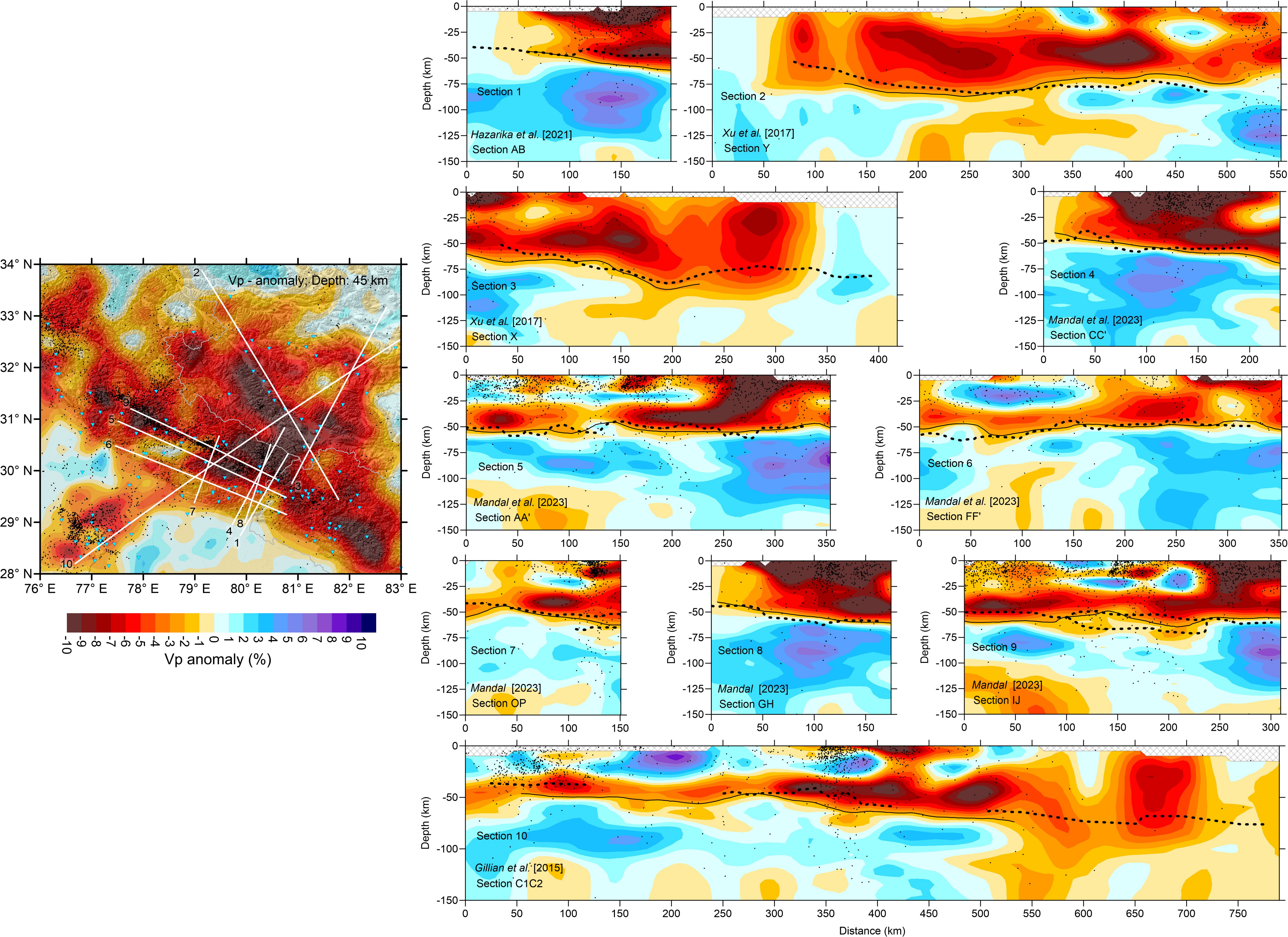

Vp - anomaly; Depth: 45 km
34° N
33° N
32° N
31° N
30° N
29° N
28° N
76° E
77° E
78° E
79° E
80° E
81° E
82° E
83° E
Vp anomaly (%)
Section 1
Hazarika et al. [2021]
Section AB
Section 2
Xu et al. [2017]
Section Y
Section 3
Xu et al. [2017]
Section X
Section 4
Mandal et al. [2023]
Section CC'
Section 5
Mandal et al. [2023]
Section AA'
Section 6
Mandal et al. [2023]
Section FF'
Section 7
Mandal [2023]
Section OP
Section 8
Mandal [2023]
Section GH
Section 9
Mandal [2023]
Section IJ
Section 10
Gillian et al. [2015]
Section C1C2
Depth (km)
Distance (km)

Figure 9: Moho Depth map and comparison with Free-Air Gravity anomalies.

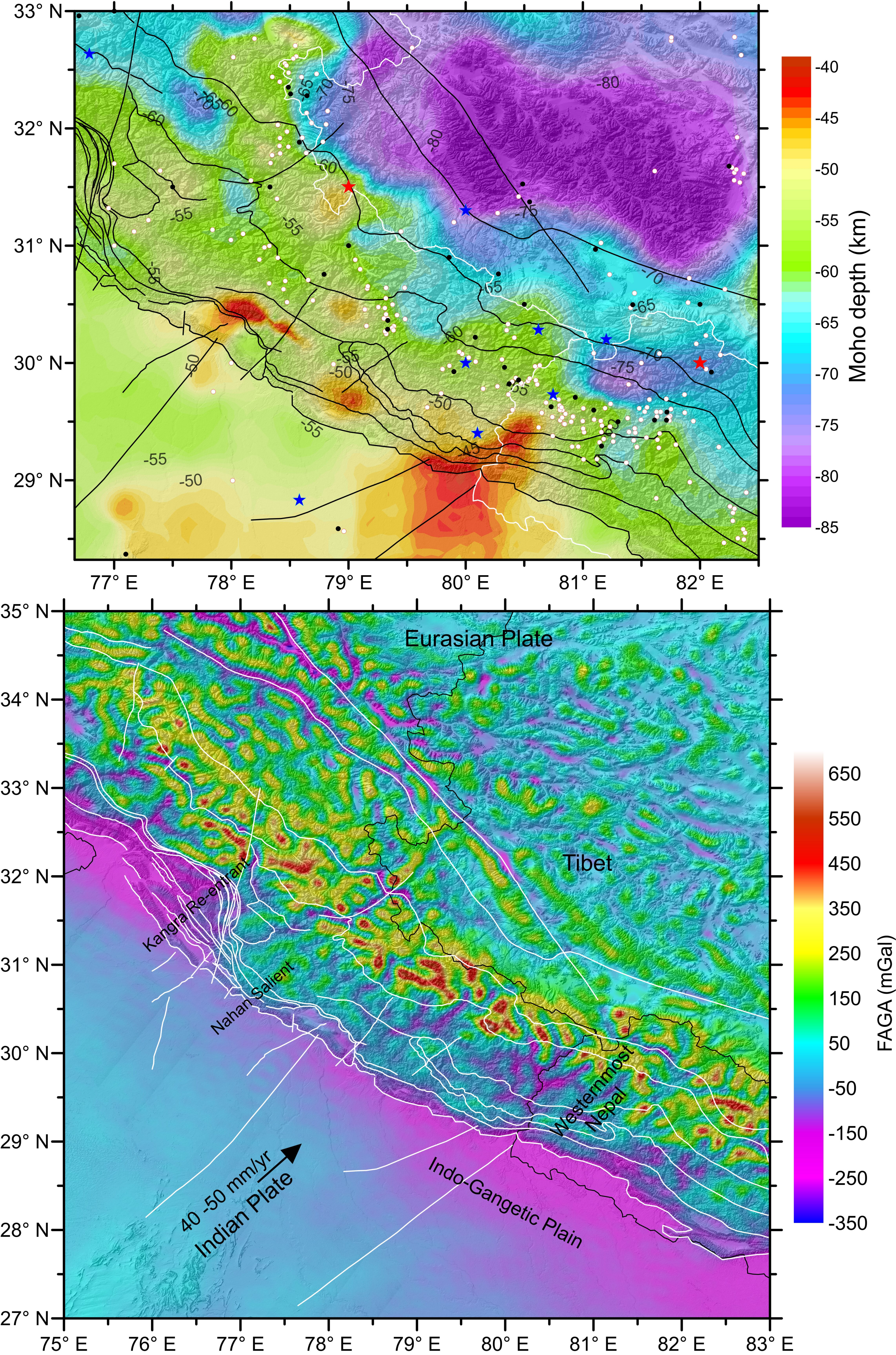

33° N
32° N
31° N
30° N
29° N
77° E
78° E
79° E
80° E
81° E
82° E
-40
-45
-50
-55
-60
-65
-70
-75
-80
-85
Moho depth (km)
35° N
34° N
33° N
32° N
31° N
30° N
29° N
28° N
27° N
75° E
76° E
77° E
78° E
79° E
80° E
81° E
82° E
83° E
Eurasian Plate
Tibet
Kangra Re-entrant
Nahan Salient
Westernmost Nepal
Indo-Gangetic Plain
40 -50 mm/yr
Indian Plate
650
550
450
350
250
150
50
-50
-150
-250
-350
FAGA (mGal)

Figure 10: Schematic representation of the Geodynamic model.

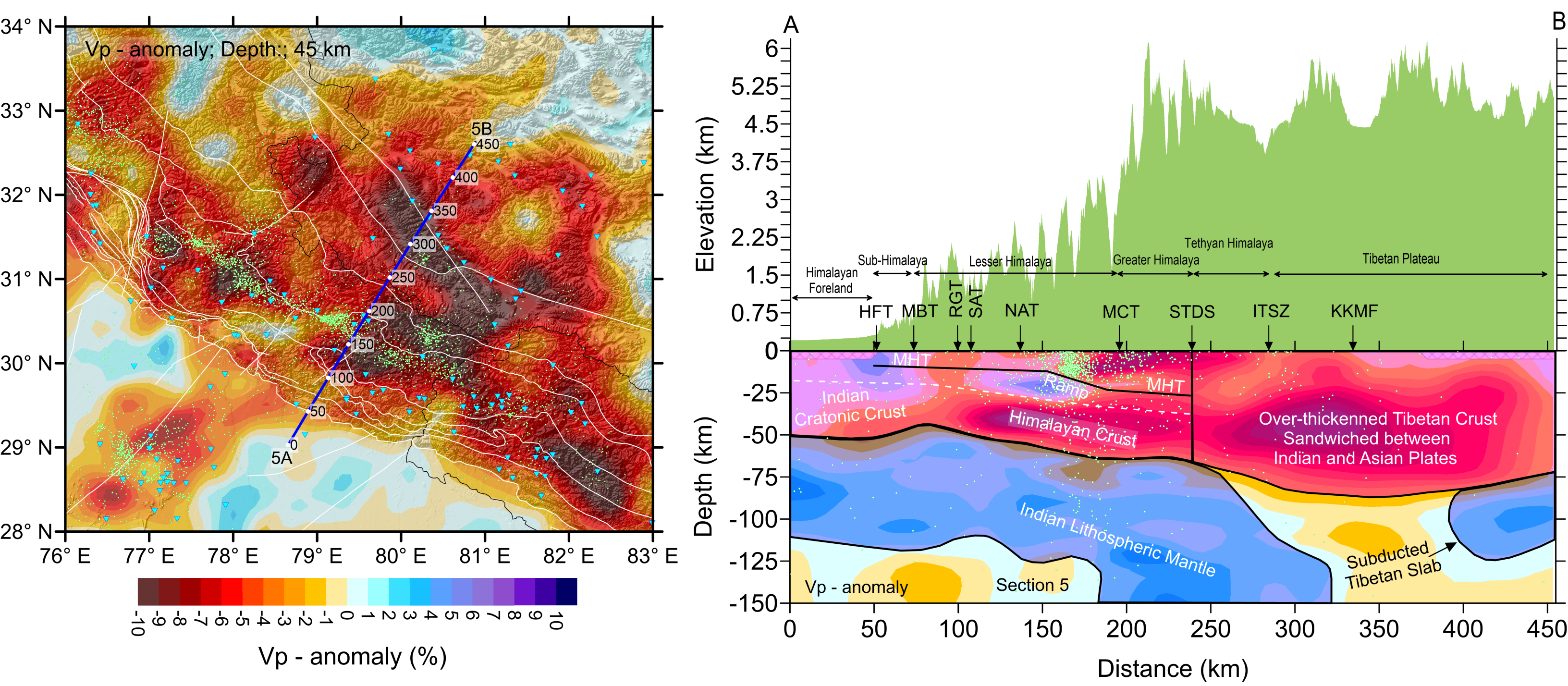

Vp - anomaly; Depth:; 45 km
5A
5B
0
50
100
150
200
250
300
350
400
450
34° N
33° N
32° N
31° N
30° N
29° N
28° N
76° E
77° E
78° E
79° E
80° E
81° E
82° E
83° E
-10 -9 -8 -7 -6 -5 -4 -3 -2 -1 0 1 2 3 4 5 6 7 8 9 10
Vp - anomaly (%)
A
B
Elevation (km)
Himalayan Foreland
Sub-Himalaya
Lesser Himalaya
Greater Himalaya
Tethyan Himalaya
Tibetan Plateau
HFT
MBT
RGT
SAT
NAT
MCT
STDS
ITSZ
KKMF
MHT
Ramp
Indian Cratonic Crust
Himalayan Crust
Over-thickenned Tibetan Crust Sandwiched between Indian and Asian Plates
Indian Lithospheric Mantle
Subducted Tibetan Slab
Vp - anomaly
Section 5
Depth (km)
Distance (km)